AD-A066 186 PURDUE UNIV LAFAYETTE IND RAY W HERRICK LABS F/G 20/4
VELOCITY AND FOLDOVER OF THE TURBULENT NON-TURBULENT INTERFACE --ETC(U)
SEP 75 D J MULEJ, V W GOLDSCHMIDT N00014-75-C-1048
UNCLASSIFIED HL-75-32 NL

1 OF 2
ADA
066186

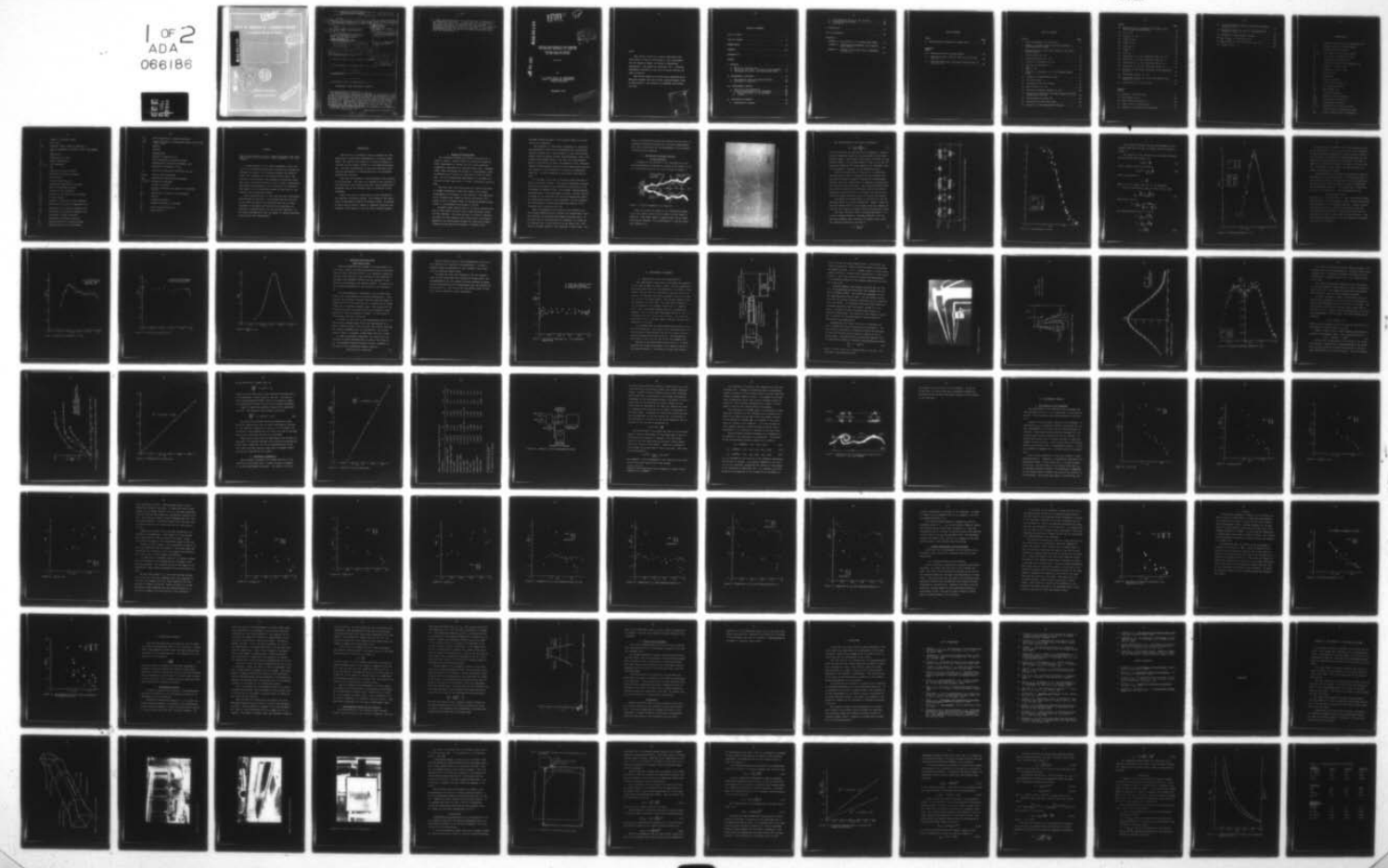

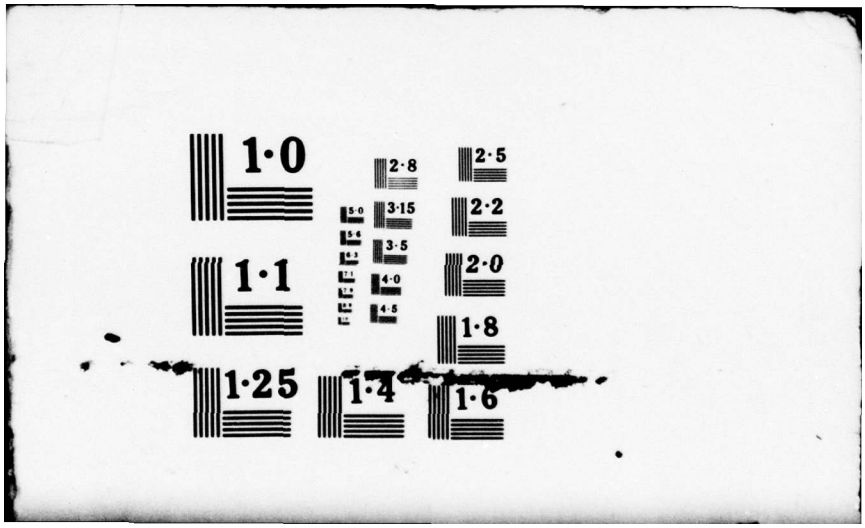
1·0
1·1
1·25
1·4
1·6
1·8
2·0
2·2
2·5
2·8
3·15
3·5
4·0
4·5
5·0

A Graduate Research Facility

PURDUE UNIVERSITY

Lafayette, Indiana 47907

SECURITY CLASSIFICATION OF THIS PAGE (When Data Entered)

REPORT DOCUMENTATION PAGE

READ INSTRUCTIONS BEFORE COMPLETING FORM

1. REPORT NUMBER
2. GOVT ACCESSION NO.
3. RECIPIENT'S CATALOG NUMBER

(6) 4. TITLE (and Subtitle)
Velocity and Foldover of the Turbulent Non-Turbulent Interface in a Plane Jet

5. TYPE OF REPORT & PERIOD COVERED
First report for Mulej's phase of work, 5/74-4/75

(14) 6. PERFORMING ORG. REPORT NUMBER
HL-75-32

7. AUTHOR(s)
(10) D.J. Mulej and V.W. Goldschmidt

8. CONTRACT OR GRANT NUMBER(s)
(15) ~~N00014-75-C-1148~~ NSF-GK-19317

9. PERFORMING ORGANIZATION NAME AND ADDRESS
School of Mechanical Engineering
R. W. Herrick Laboratories
Purdue University
~~West Lafayette, IN 47907~~

10. PROGRAM ELEMENT, PROJECT, TASK AREA & WORK UNIT NUMBERS
NR062-497

11. CONTROLLING OFFICE NAME AND ADDRESS
Fluid Dynamics, Mathematical & Information Sciences Division, Office of Naval Research
800 N. Quincy Street, Arlington, Va. 22217

12. REPORT DATE
Sept. 1975
Distributed 2/1979

13. NUMBER OF PAGES
104

14. MONITORING AGENCY NAME & ADDRESS (if different from Controlling Office)

15. SECURITY CLASS. (of this report)
Unclassified

15a. DECLASSIFICATION/DOWNGRADING SCHEDULE
N/A

(9) Rept. no. 1, May 74 - Apr 75

16. DISTRIBUTION STATEMENT (of this Report)

(11) Sep 75

Approved for public release; distribution unlimited.

(12) 106p.

17. DISTRIBUTION STATEMENT (of the abstract entered in Block 20, if different from Report)

18. SUPPLEMENTARY NOTES

19. KEY WORDS (Continue on reverse side if necessary and identify by block number)

Turbulence, Jets, Interface, Foldover

20. ABSTRACT (Continue on reverse side if necessary and identify by block number)

A unique measure of the lateral component of the velocity of the turbulent-nonturbulent interface was defined and expressed in terms of the crossing frequency and intermittency, both parameters of the turbulent flow field. The velocity of the interface was compared for different turbulent shear flows and was found to show a trend of similarity. Experimental measurements of the velocity of the interface were taken in a two dimensional plane jet and found to correspond with the predicted values. —over (over)

DD FORM 1 JAN 73 1473 EDITION OF 1 NOV 65 IS OBSOLETE
S/N 0102-014-6601

SECURITY CLASSIFICATION OF THIS PAGE (When Data Entered)

407 205

JOB

20. Other characteristics of the interface were investigated and reported in this work. It was noted that the velocity of the front and back of the interface were not the same. A measure of the amount of folding in the interface as a function of location within the jet was also reported. It was found experimentally that the amount of folding increases directly with the intermittency.

VELOCITY AND FOLDOVER OF THE TURBULENT NON-TURBULENT INTERFACE IN A PLANE JET

Prepared Under NSF GK19317
and ONR N00014-67-A-0226

HL 75-32

by

D. J. Mulej and V. W. Goldschmidt
School of Mechanical Engineering
Purdue University

September 1975

Note:

This report is part of a thesis submitted by Mr. David Mulej in partial fulfillment of the requirements for the degree of Master of Science in Mechanical Engineering. The thesis was dated May 1975. Professor Goldschmidt assisted in this work as thesis advisor and major professor.

The initial phases of the work were sponsored by an NSF grant whereas the final effort received support from an ONR contract. The authors are indebted and grateful for both.

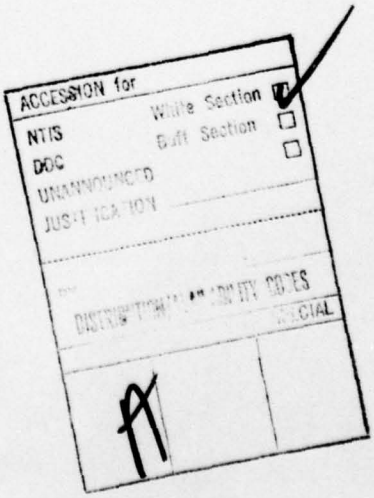

TABLE OF CONTENTS

LIST OF TABLES

LIST OF FIGURES

NOMENCLATURE

A	empirical coefficient for exponential fit
a	constant used for virtual origins
a	voltage gain in Figure B-1
b, b_u	half width of the velocity field
b_θ	half width of temperature field
b	voltage gain in Figure B-1
C	empirical constant for exponential fit
C_1	geometric virtual origin
C_2	kinematic virtual origin
c_p	specific heat
D	slot width
d	cylinder diameter
E_n	total voltage signal of n
e_n	AC voltage signal of n
e_n'	RMS voltage of n
f_γ	crossing frequency
f_{γ_m}	maximum crossing frequency
$g(r)$	lateral space correlation
$I(t)$	Intermittency function
k, k_1	widening rate of velocity field
k_2	widening rate of temperature field
Nu_d	Nusselt number based on diameter, d

n	number of turbulent bursts
Q	heat flux
Re_d	Reynolds' number based on diameter, d
r	lateral separation of probes 3 and 4 (see Figure 12)
T	temperature
T	large period of time
T_∞	ambient temperature
Δt, t_{ij}	time increments
t	time
U	velocity in axial direction
U_m	maximum or centerline velocity
U_o	exit velocity
U_1	velocity defect ($U_m - U$)
u	fluctuating component of velocity
u'	RMS of fluctuating velocity
V_i	velocity of the interface
V_{bi}	velocity of the back of the interface
V_{dc}	DC bias voltage
V_{fi}	velocity of the front of the interface
V_{i1}	definition of V_i given by Equation (11)
V_{i2}	definition of V_i given by Equation (12)
V_{i3}	definition of V_i given by Equation (13)
x	coordinate in axial direction
y	coordinate in lateral direction
y_d	lateral position of detector probes
y_i	lateral position of the interface

Δy	probe separation in lateral direction
Δy^*	measure of width of intermittent region ($y(\gamma = 0.01) - y(\gamma = 0.99)$)
α	$\sqrt{\ln 2}/b_u$
β	$\sqrt{\ln 2}/b_\theta$
γ	intermittency
γ	$\sqrt{\alpha^2 + \beta^2}$ in Equation A-14
δ	probe separation of detector probes
η	nondimensional similarity variable, $\sigma y/x$
θ	temperature difference, $T - T_\infty$
θ_m	centerline temperature difference, $T_m - T_\infty$
Λ, Λ_g	lateral space macroscale
Λ_{g1}	approximate lateral space macroscale
$(\nu^3/\epsilon_o)^{\frac{1}{4}}$	Kolmogorov microscale
ν	kinematic viscosity
ξ	lateral coordinate with respect to interface $(y_d - y)$
ϕ_i	percentage of folding in the interface
ρ	density
σ	standard deviation
σ_m	standard deviation of the mean
$\hat{q}$	point averaged value of q
$\bar{q}$	mean value of q

ABSTRACT

Mulej, David Joseph, M. S. M. E., Purdue University, May, 1975. The Velocity of the Interface. Major Professor: V. W. Goldschmidt.

A unique measure of the lateral component of the velocity of the turbulent-nonturbulent interface was defined and expressed in terms of the crossing frequency and intermittency, both parameters of the turbulent flow field. The velocity of the interface was compared for different turbulent shear flows and was found to show a trend of similarity. Experimental measurements of the velocity of the interface were taken in a two dimensional plane jet and found to correspond with the predicted values.

Other characteristics of the interface were investigated and reported in this work. It was noted that the velocity of the front and back of the interface were not the same. A measure of the amount of folding in the interface as a function of location within the jet was also reported. It was found experimentally that the amount of folding increases directly with the intermittency.

INTRODUCTION

This work is a continuation and an outgrowth of work being done in conditional measurements of turbulent shear flows. The work by this author is a natural extension of the work by Pete Jenkins (1974) in a two dimensional plane jet. The main investigation in this work concerns itself with the measurement of characteristics of the turbulent-nonturbulent interface.

This work will present a unique measure of the velocity of the interface. This will be a measure of the velocity of the interface in the lateral direction, which constitutes a different view of the interface than is currently in the literature.

There will also be a discussion of other measures of the interface including folding. The folding of the interface, as discussed by Paizis and Schwarz (1974), is defined as the action by which a region of turbulent fluid has nonturbulent fluid between it and the fully turbulent region.

I ANALYSIS

1. Review of Previous Work

The turbulent interface has been investigated for a number of years. Corrsin (1943) is credited as being the first investigator to observe via a hot wire probe the intermittent character of a turbulent shear flow. Townsend (1948, 1949) introduced the concept of intermittency, which is defined as the fraction of time that the flow is turbulent. He took intermittency measurements in the wake of a circular cylinder and found it to obey a similarity relationship.

The first major work discussing the interface was that of Corrsin and Kistler (1954) which among other things investigated the thickness of the interface. The superlayer, as the interface was termed by Corrsin and Kistler, was found to have a thickness based on similarity grounds proportional to the Kolmogorov microscale, $(\nu^3/\epsilon_o)^{\frac{1}{4}}$.

Townsend (1956) compiled much of the early intermittency data in free shear flows and later (1966) proposed a model for the interface. His intention was to propose a theoretical model for the interface that would explain its behavior, especially the relationship between the interface's highly irregular nature and the entrainment of ambient fluid.

Townsend thereby proposed a visco-elastic model for the motion of the interface.

The technique of conditional averaging is a relatively new experimental method for investigating the intermittent regions of shear flow. Early workers in this field include Kibens (1968), Kovasznay, Kibens, and Blackwelder (1970), and Jenkins (1974) among others. The basis for these measurements is the ability to detect the presence of the interface. Jenkins (1974) measured the velocity and temperature profiles with respect to the interface in a heated two dimensional plane jet. He also presented an up-to-date literature review.

Of interest is the work of Phillips (1972) and that of Paizis and Schwarz (1974). Phillips was primarily concerned with the part played by the interface in the action of the entrainment of ambient fluid. He proposed a pseudo-Lagrangian description of the entrainment process. Paizis looked at the shape of the interface and noted the significant amount of folding which occurs in the interface. He also measured the characteristic scales and convection velocity of the interface for a turbulent wall jet.

Most investigators have looked at the interface as a thin surface separating the turbulent and nonturbulent flows. That surface is convected downstream by the mean flow. In the work that is now presented the interface in a plane jet is observed from a fixed position in the shear flow. The relative lateral motion of the interface is then noted. The

motion is periodically inward and outward from the point of reference (without accounting for the axial displacement). This view is the basis for the measurement of the (lateral) velocity of the interface.

2. Derivation of Lateral Velocity of the Interface

A measure of the velocity of the interface as it has been developed may be gained by looking at the output of two hot wire probes placed in the flow as shown in Figure 1.

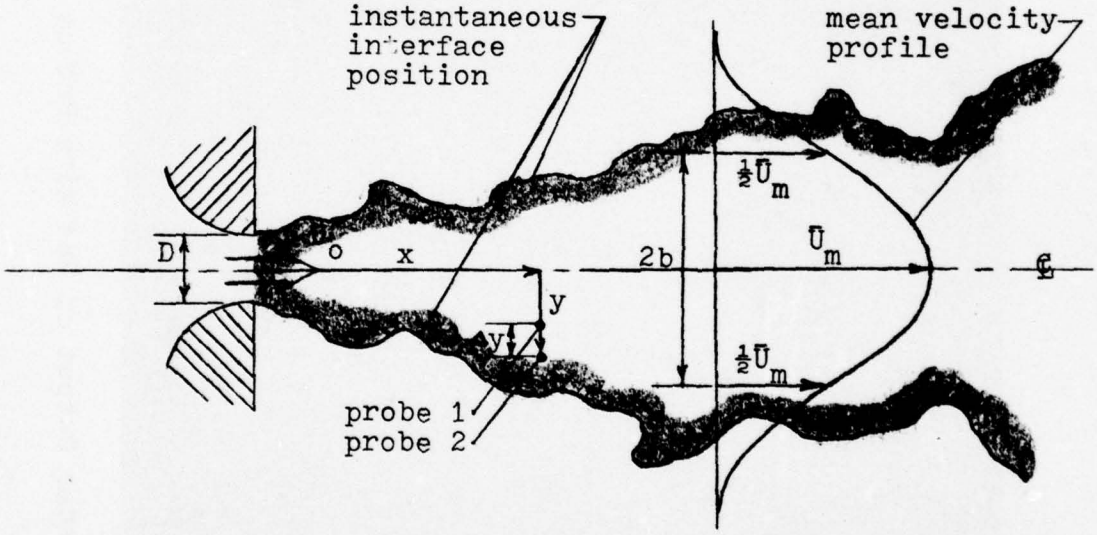

Figure 1 Probe Arrangement in a Plane Jet

When the probes are placed in the intermittent region of the jet, their output will be similar to that shown in Figure 2. From these types of signals there are two terms which may be defined: the intermittency, γ, and the crossing frequency, f_γ.

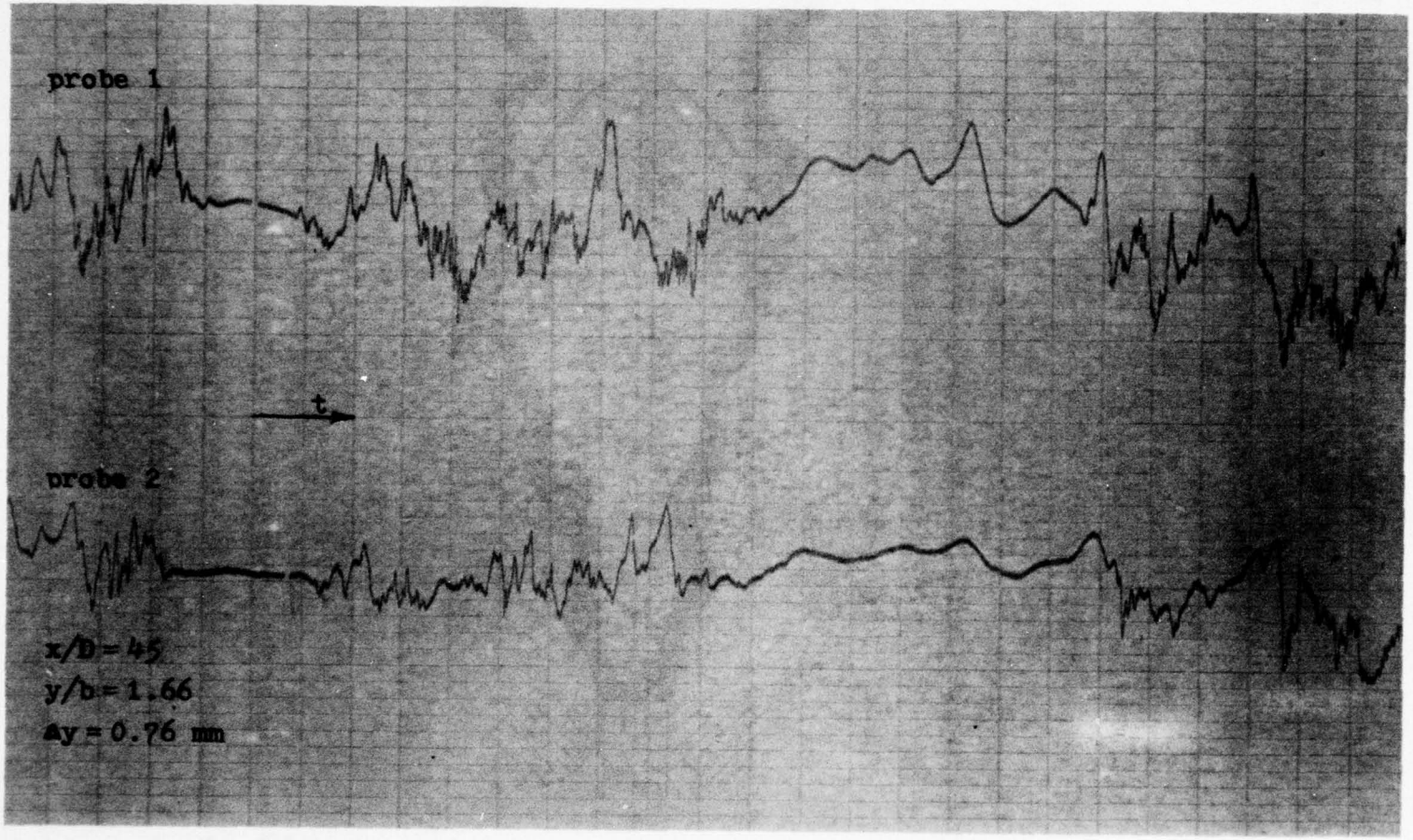

Figure 2 Sample Visicorder Output of Hot Wire Probes in the Intermittent Region

The intermittency of the flow is defined as

$$\gamma_i = \lim_{T \to \infty} \frac{1}{T} \sum_{j=1}^{n} t_{ij} \qquad (1)$$

or as the fraction of time the flow is turbulent. Figure 3 shows an idealized output of hot wire probes in the intermittent region. From Figure 3 the terms of Equation (1) are clearly shown: T is a large period of time, t_{ij} is the j^{th} portion of time the i^{th} trace appears to be turbulent, and n is the number of turbulent bursts during the time T.

Using the traces shown in Figure 2 it is relatively obvious when the flow is turbulent and nonturbulent, and also quite straight forward to measure the intermittency. However, when the intermittency is measured electronically, the problem is more difficult. Any electronic method which may be used to measure intermittency, such as the method described by Jenkins (1974), is usually verified and calibrated by using visicorder traces of the hot wire probes.

At present the intermittency of the flow in a two dimensional plane jet is well understood. Figure 4 shows the data by Jenkins (1974) in the present setup and compares it with the data taken by Bradbury (1965) and Heskestad (1965).

The other term which may be deduced from Figure 2 or 3 is the crossing frequency, sometimes referred to as the bursting frequency when speaking of boundary layer flows. The crossing frequency is defined as

$$f_\gamma = \lim_{T \to \infty} \frac{n}{T} \qquad (2)$$

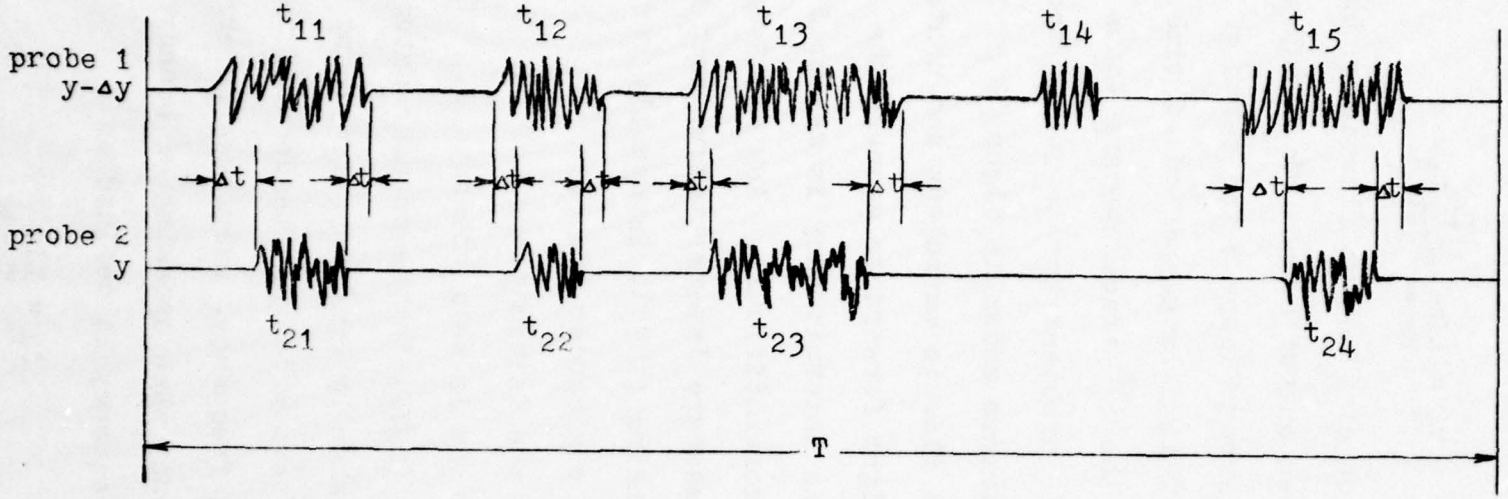

Figure 3 Idealized Output of Hot Wire Probes in the Intermittent Region

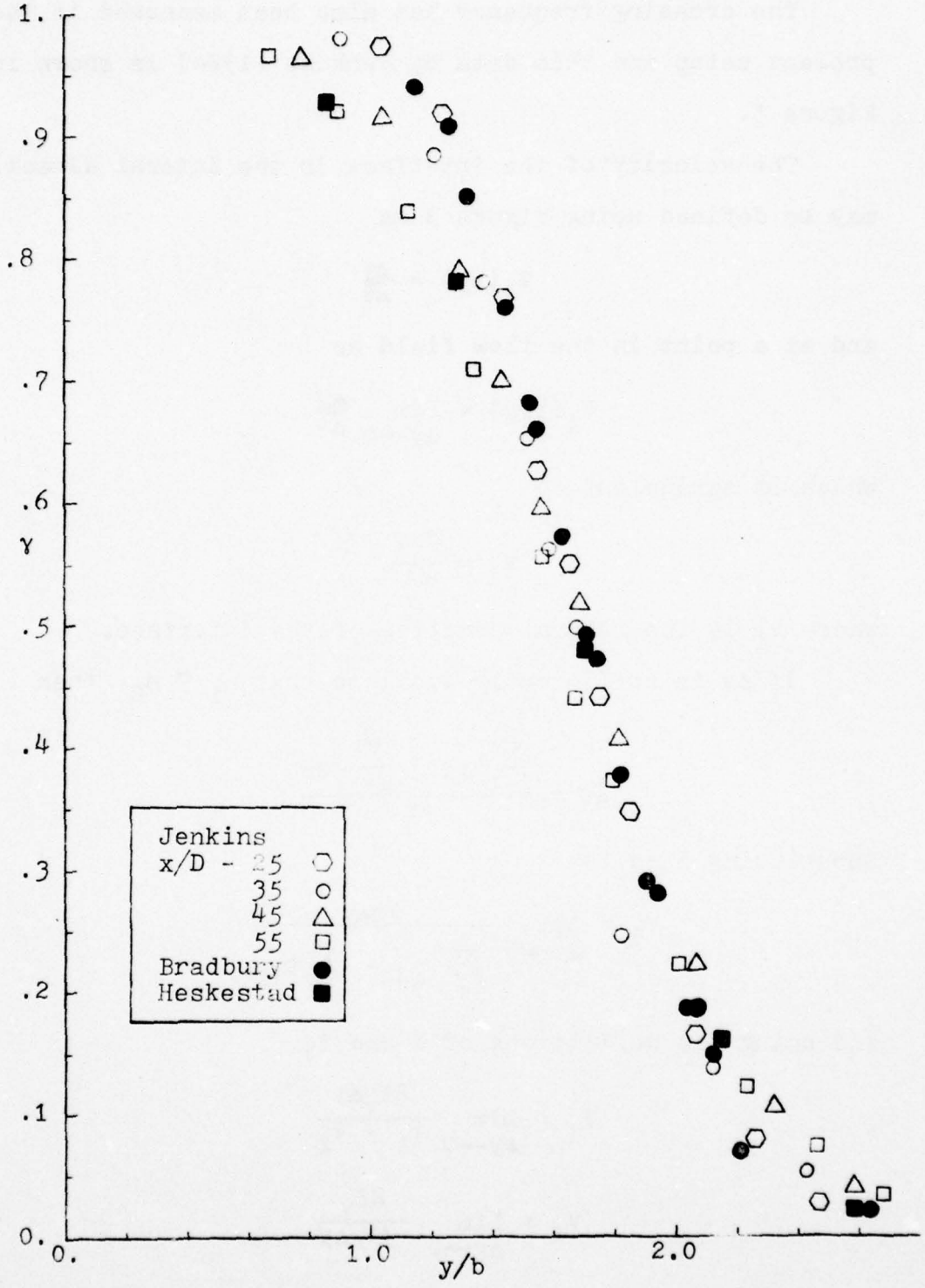

Figure 4 Intermittency vs. y/b

The crossing frequency has also been measured in the present setup and this data by Jenkins (1974) is shown in Figure 5.

The velocity of the interface in the lateral direction may be defined using Figure 3 as

$$V_i(\Delta y) = \frac{\Delta y}{\Delta t} \tag{3}$$

and at a point in the flow field as

$$V_i(x,y) = \lim_{\Delta y \to 0} \frac{\Delta y}{\Delta t} \tag{4}$$

which is equivalent to

$$V_i = \frac{dy_i}{dt}$$

where y_i is the lateral position of the interface.

If Δy is sufficiently small so that $n_1 \cong n_2$, then

$$\overline{\Delta t} = \frac{\sum_{j=1}^{n} t_{1j} - \sum_{k=1}^{n} t_{2k}}{2n} \tag{5}$$

Substituing into (4)

$$V_i = \lim_{\Delta y \to 0} \frac{2n\Delta y}{\sum_{j=1}^{n} t_{ij} - \sum_{k=1}^{n} t_{ik}}$$

and using the definitions of γ and f_γ

$$V_i = \lim_{\Delta y \to 0} \frac{2f_\gamma \Delta y}{\gamma_1 - \gamma_2}$$

$$V_i = \lim_{\Delta y \to 0} \frac{2f_\gamma}{-\Delta\gamma/\Delta y}$$

$$V_i = \frac{-2f_\gamma}{\partial\gamma/\partial y} \tag{6}$$

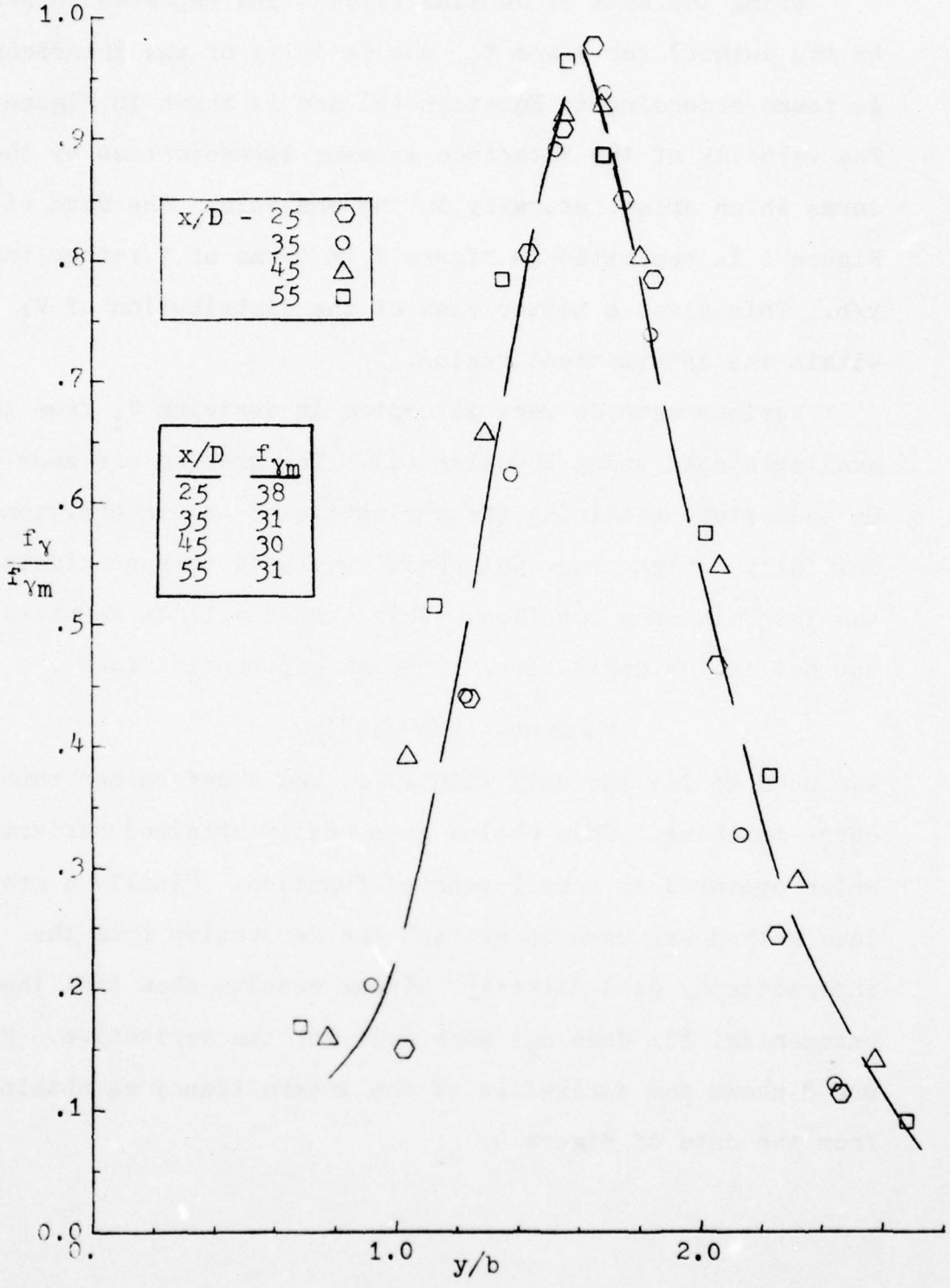

Figure 5 Crossing Frequency vs. y/b

Using the data of Jenkins (1974) (and repeated in part by the author) for γ and f_γ, the velocity of the interface is found according to Equation (6) and is shown in Figure 6. The velocity of the interface is made dimensionless by the terms which arise naturally in the analysis. The data of Figure 6 is replotted in Figure 7 in terms of γ rather than y/b. This gives a better view of the distribution of V_i within the intermittent region.

Various methods were attempted in deriving V_i from the available data using Equation (6). The problem was seen to be accurately obtaining the derivative of the intermittency. Initially a high order polynomial was used to approximate the intermittency function. This agreed well in magnitude, but not in the derivative. Then an exponential form

$$\gamma = \exp(-A(y/b - c)^n)$$

was used to fit the data with A, c, and n determined through curve matching. This choice gave easily obtained derivatives which appeared as a well behaved function. Finally a graphical method was used to extract the derivative from the intermittency data directly. These results show that the exponential fit does not work well for the derivative. Figure 8 shows the derivative of the intermittency as obtained from the data of Figure 4.

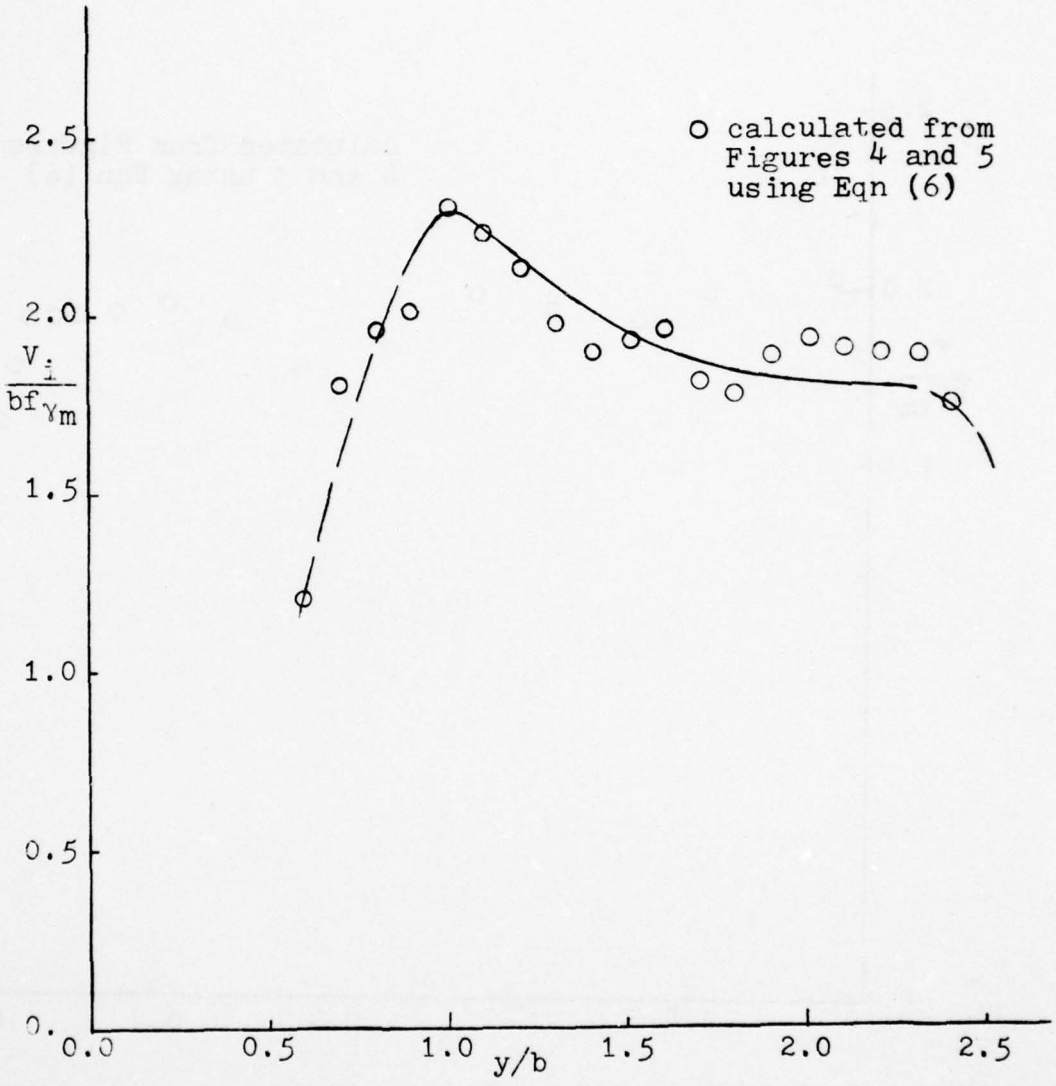

Figure 6 Velocity of Interface vs. y/b

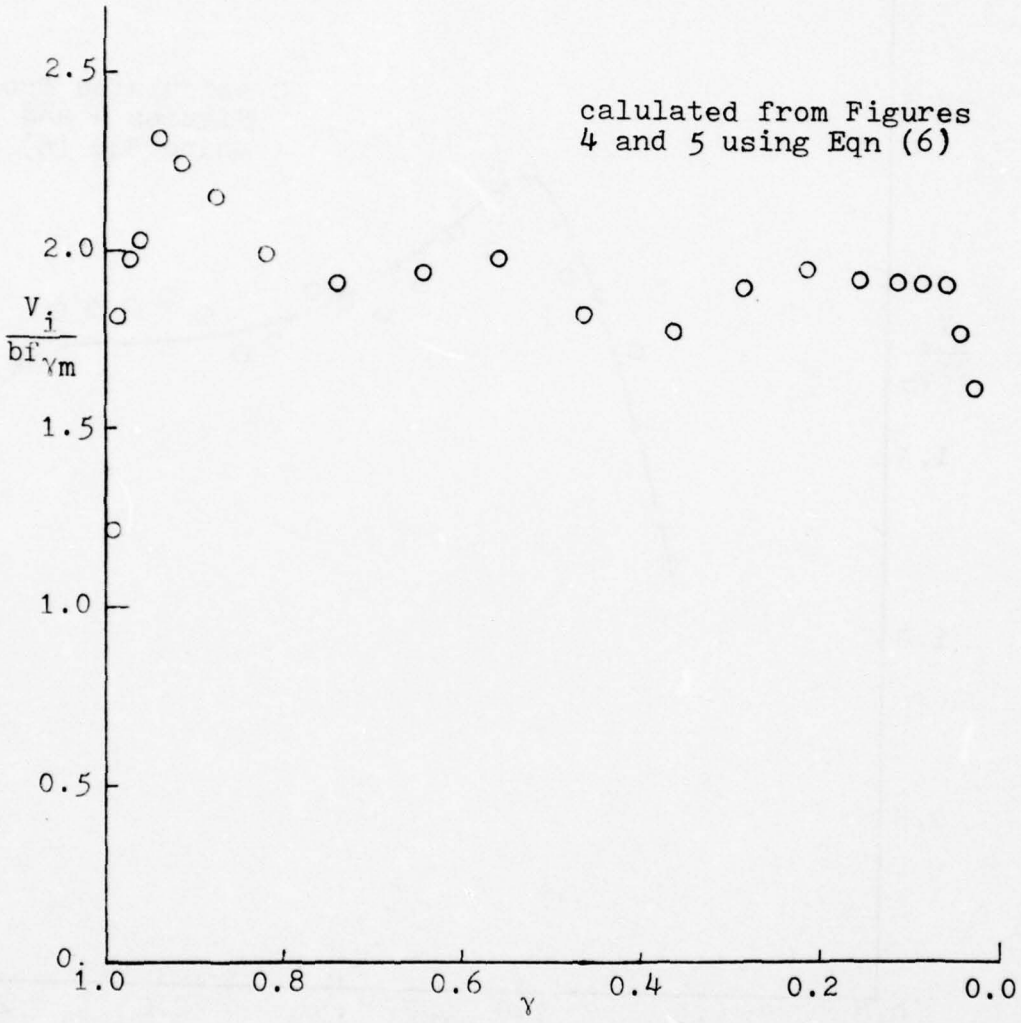

Figure 7 Velocity of Interface vs. γ

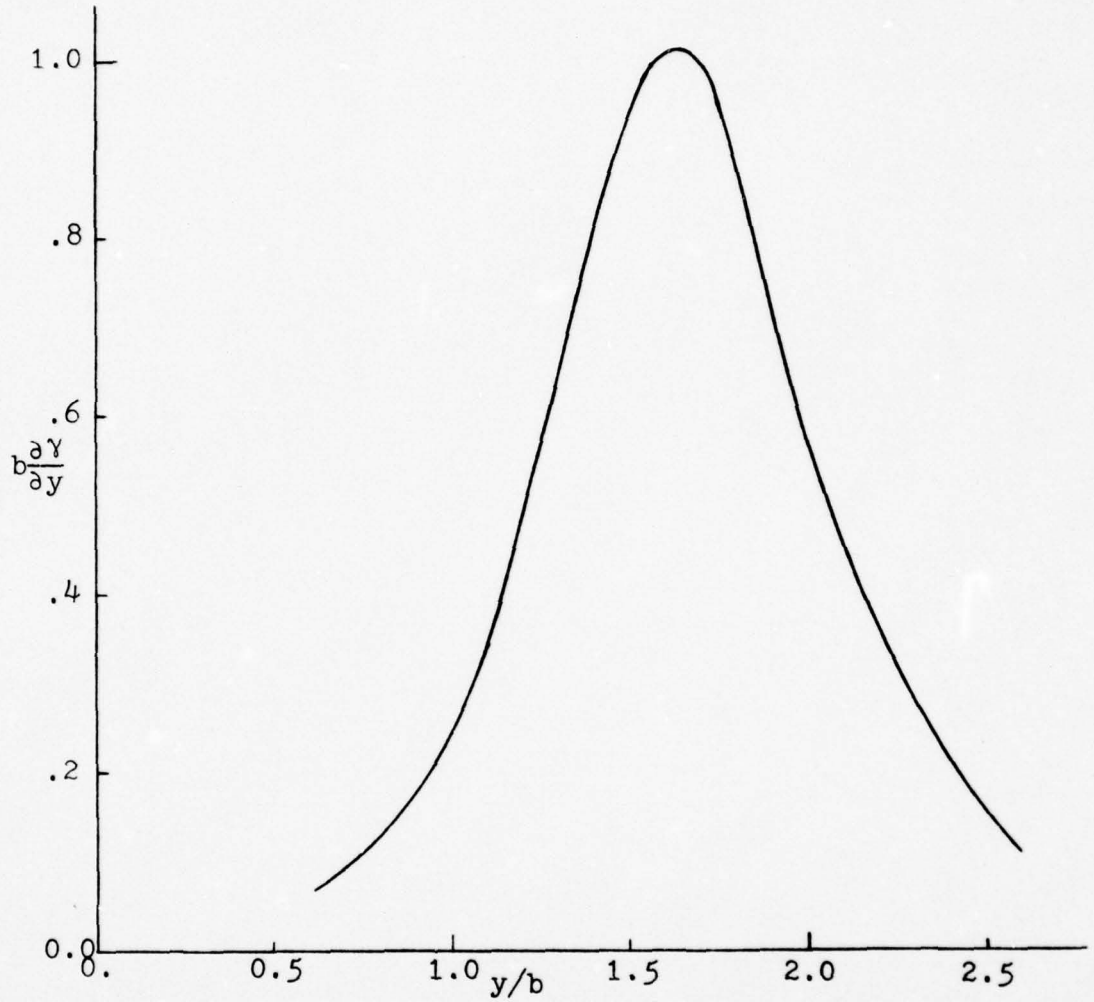

Figure 8 $b\frac{\partial \gamma}{\partial y}$ vs. y/b

3. Comparison With Data From Other Shear Flows

Earlier researchers have spoken of an entrainment velocity (the velocity at which nonturbulent fluid is entrained into the flow, Phillips (1972)), of an interface convection velocity (the velocity of the interface in the direction of the mean flow, Bradshaw (1967)), and the velocity of the fluid at the interface (see Jenkins (1974)). Of concern now is the lateral component of the velocity of the interface, V_i.

The data necessary to determine V_i can be found from other shear flows measured by earlier investigators. Intermittency and crossing frequency data have been published by Thomas (1973) for the plane wake of a cylinder and by Kibens (1968) for a turbulent boundary layer. The velocity of the interface has been calculated from this information using Equation (6) and is compared in Figure 9 to that found in this present work for a plane jet.

In order to solve for V_i the intermittency data for the wake and the boundary layer were first approximated by a smooth function chosen to fit the data (but without checking for complete agreement with the derivative). The points shown in Figure 9 represent values taken from the f_γ data.

To make a meaningful comparison, the velocity of the interface was made nondimensional in each of the flows by $f_{\gamma m}$, the maximum crossing frequency and Δy^*, a measure of the width of the intermittent region, given by

$$\Delta y^* = y(\gamma=0.01) - y(\gamma=0.99) \qquad (7)$$

Figure 9 shows a plot of the nondimensional velocity of the interface as a function of intermittency. It shows a definite trend of similarity in the velocity of the interface for different shear flows.

It should be noted that although V_i for the boundary layer and the plane wake were obtained as stated above, the corresponding V_i for the current work was obtained by graphically differentiating the intermittency data and reading off the values of f_γ. It is felt that the results shown in Figure 9 are not affected by this difference.

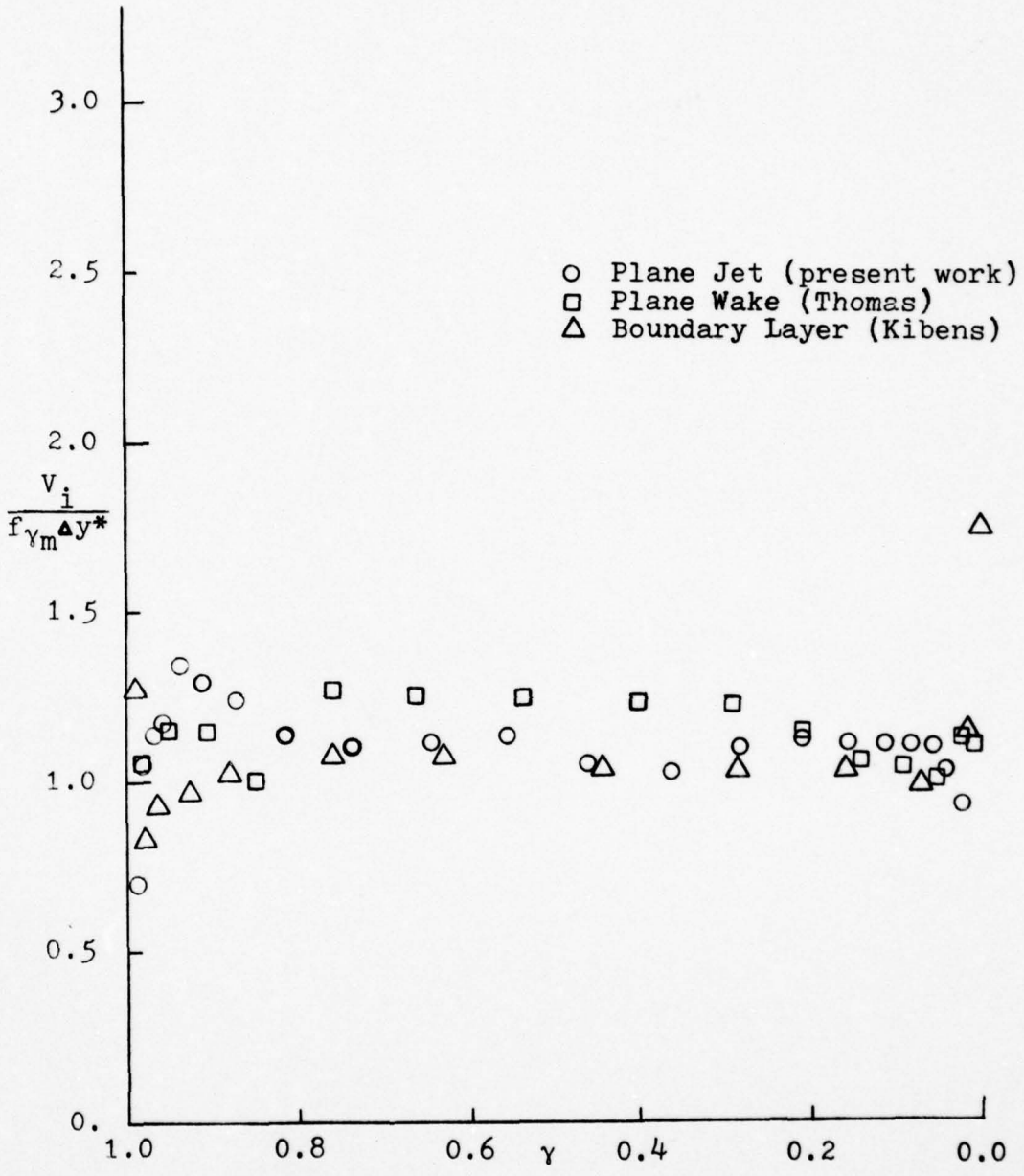

Figure 9 Velocity of Interface vs. γ for Different Shear Flows

II EXPERIMENTAL PROCEDURE

1. Experimental Setup and Characteristics

The experimental setup used for this work was essentially the same as used by Jenkins (1974). The two dimensional plane jet (see Figure 10) was powered by a 0.56 kW (0.75 hp) blower. The jet has the capability of heating the flow by use of a 4.0 kW mesh wire heating element, which is located in a 56 x 51 cm plenum chamber. The heating capability was not necessary for this work. From the plenum chamber the flow is directed via a gradual contraction to a smaller (15.2 x 30.4 cm) plenum chamber with flow straightening elements. The flow was then discharged through a 1.27 x 30.4 cm vertical slot on a 91.4 x 30.4 cm wall. Two horizontal walls (91.4 x 121.0 cm) were used to maintain the two dimensionality of the flow.

A two dimensional traversing mechanism was used to move the probe apparatus. The range of the traversing device was 60 slot-widths longitudinally and 44 slot-widths laterally, with an accuracy better than ±0.04 cm. The measurements were taken at $x/D = 35$, 45, and 55 for this present work.

Mounted on the probe support mount was an L. C. Smith actuator that permitted movement of the sampling probes in the lateral direction. The detector probes were movable

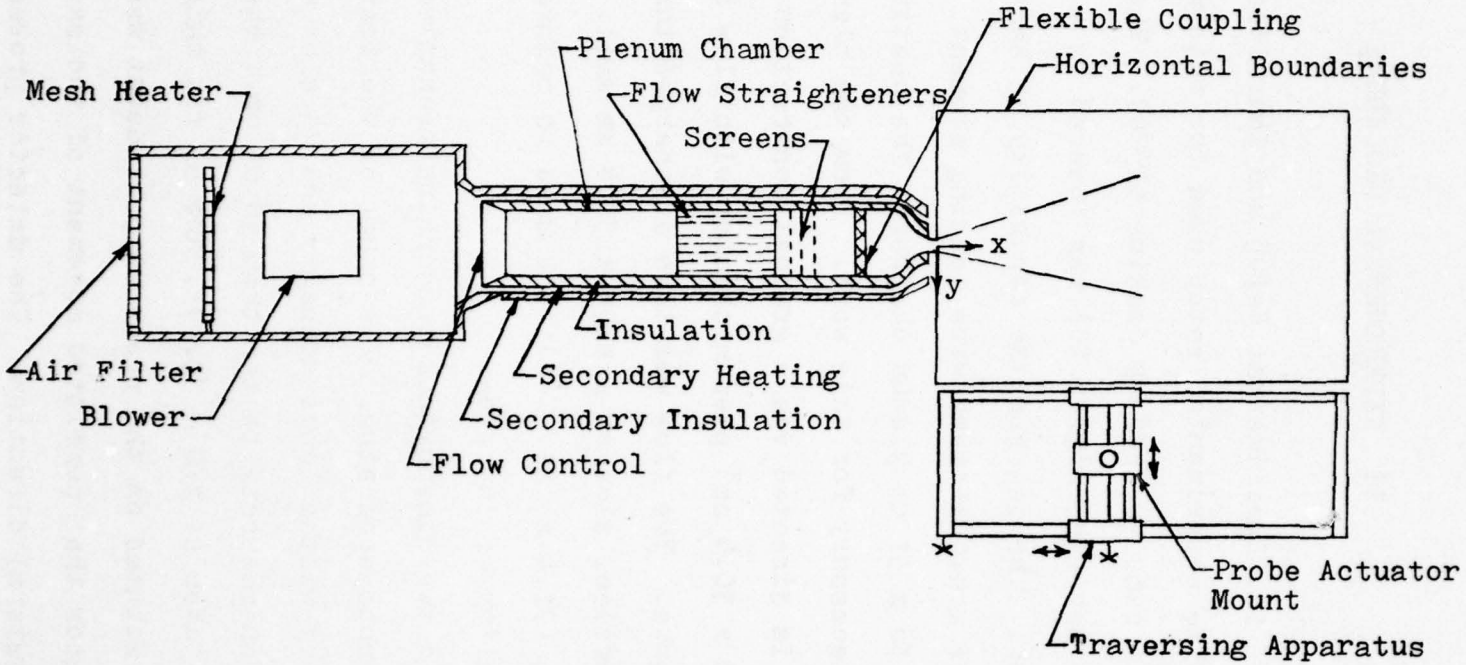

Figure 10 Schematic of Experimental Setup

only by moving the probe support mount. The actuator provided an electrical, remote controlled method of traversing the sampling probes. A D.C. voltage across a 10-turn potentiometer provided a voltage output proportional to the lateral traverse. The total available traverse was approximately 30 slot-widths relative to the actuator mount with an accuracy of ±0.02 cm.

The probe support (see Figures 11 and 12) was the only part of the experimental setup which was changed from that used by Jenkins (1974). The change was necessary so that two sampling probes could be used. The two probes could be moved (in the lateral direction, manually) up to a separation of 8 slot-widths. The sampling probes were also limited to a maximum separation from the detector probes of 5 slot-widths. Neither of these constraints were found to be adversely restrictive. The purpose of this change in design was to provide for the measurement of space-correlation coefficients (see Appendix B).

Measurements were taken in the jet to determine how well it agreed with work from previous investigators. The mean velocity and relative intensity profiles were measured at three x/D stations and are shown in Figures 13 and 14 respectively. The mean velocity profile was compared with the theoretical results of Goertler (from Schlichting (1968))

$$\frac{\bar{U}}{\bar{U}_m} = 1 - \tanh^2 \eta \qquad (8)$$

where $\eta = \sigma y/x$, and σ is a characteristic of the jet. For this work σ was found to be 9.28.

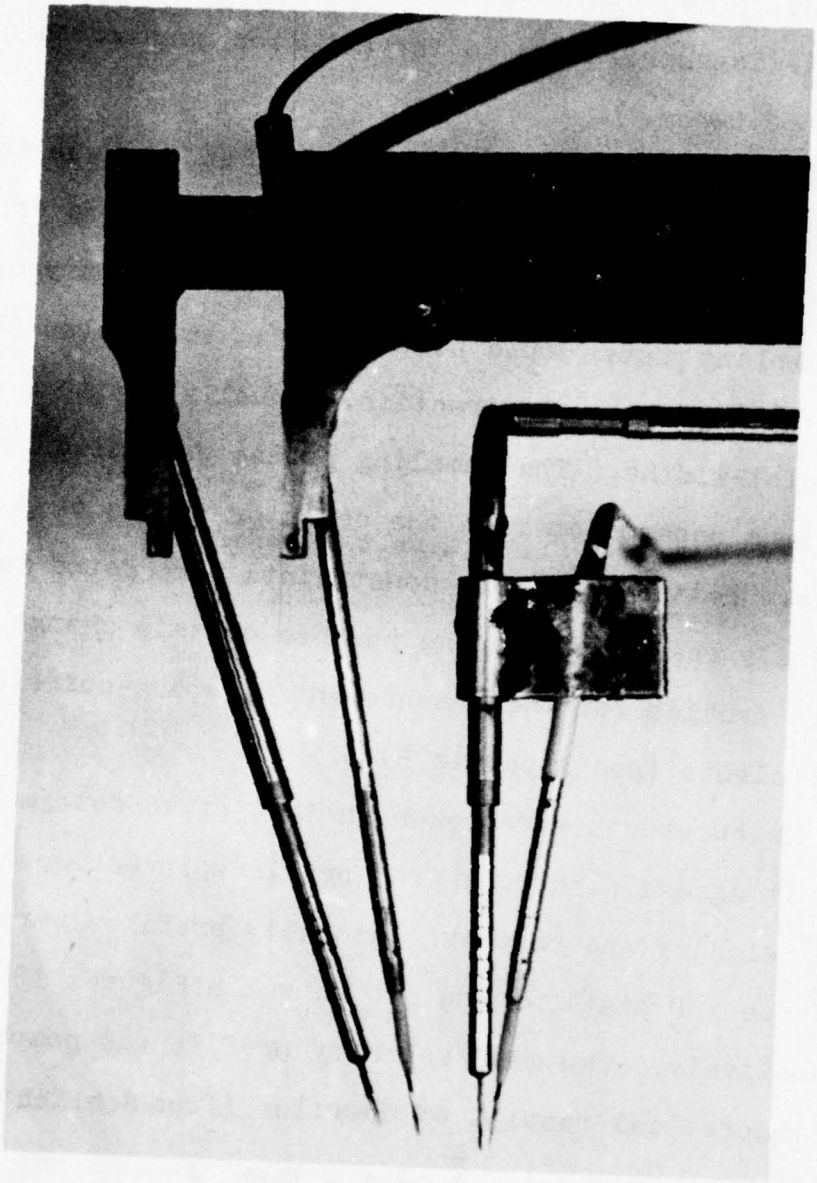

Figure 11 Hot Wire Probes

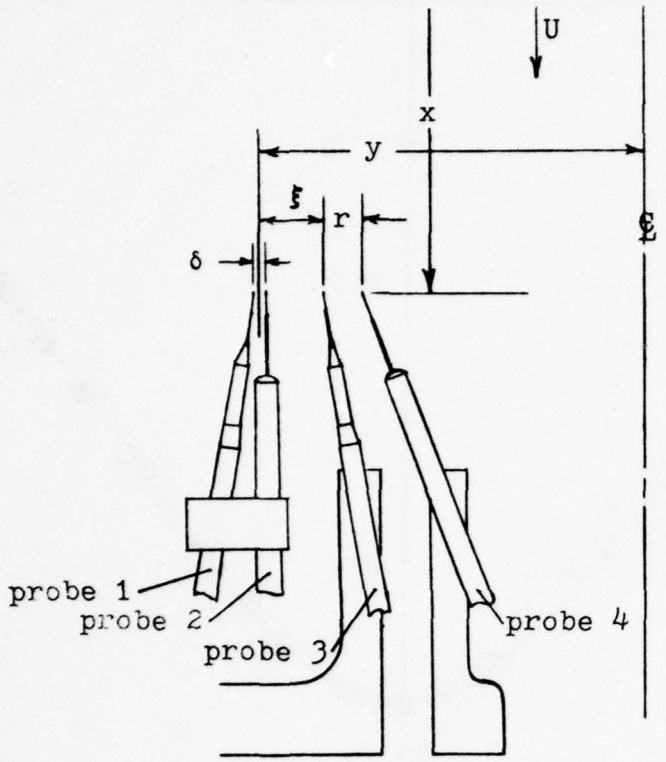

δ = 1.5 mm

$1.5 \geq \xi \leq 66.0$ mm

$1.3 \geq r \leq 110.0$ mm

Figure 12 Schematic of Hot Wire Probes

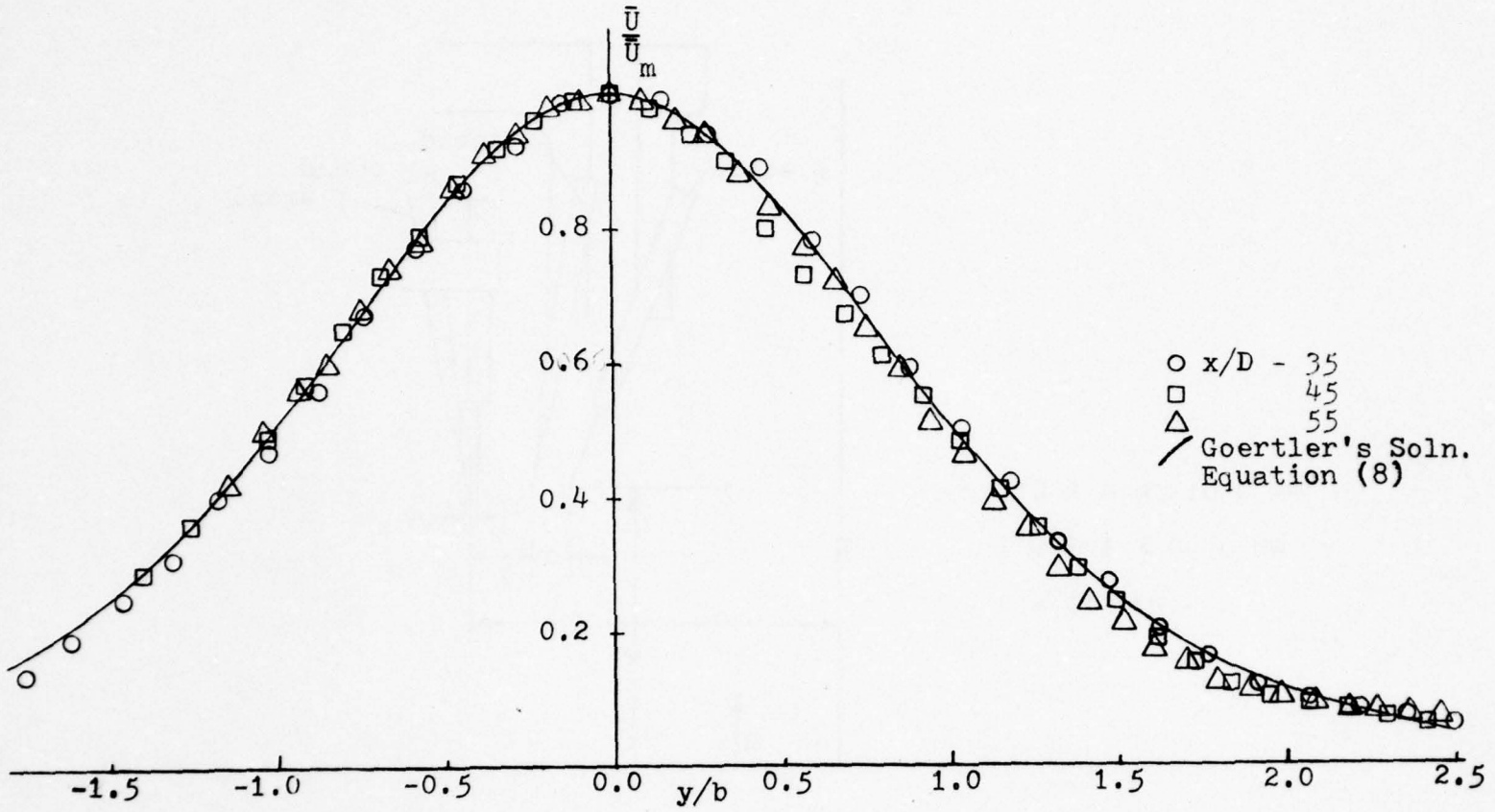

Figure 13 Mean Velocity vs. y/b

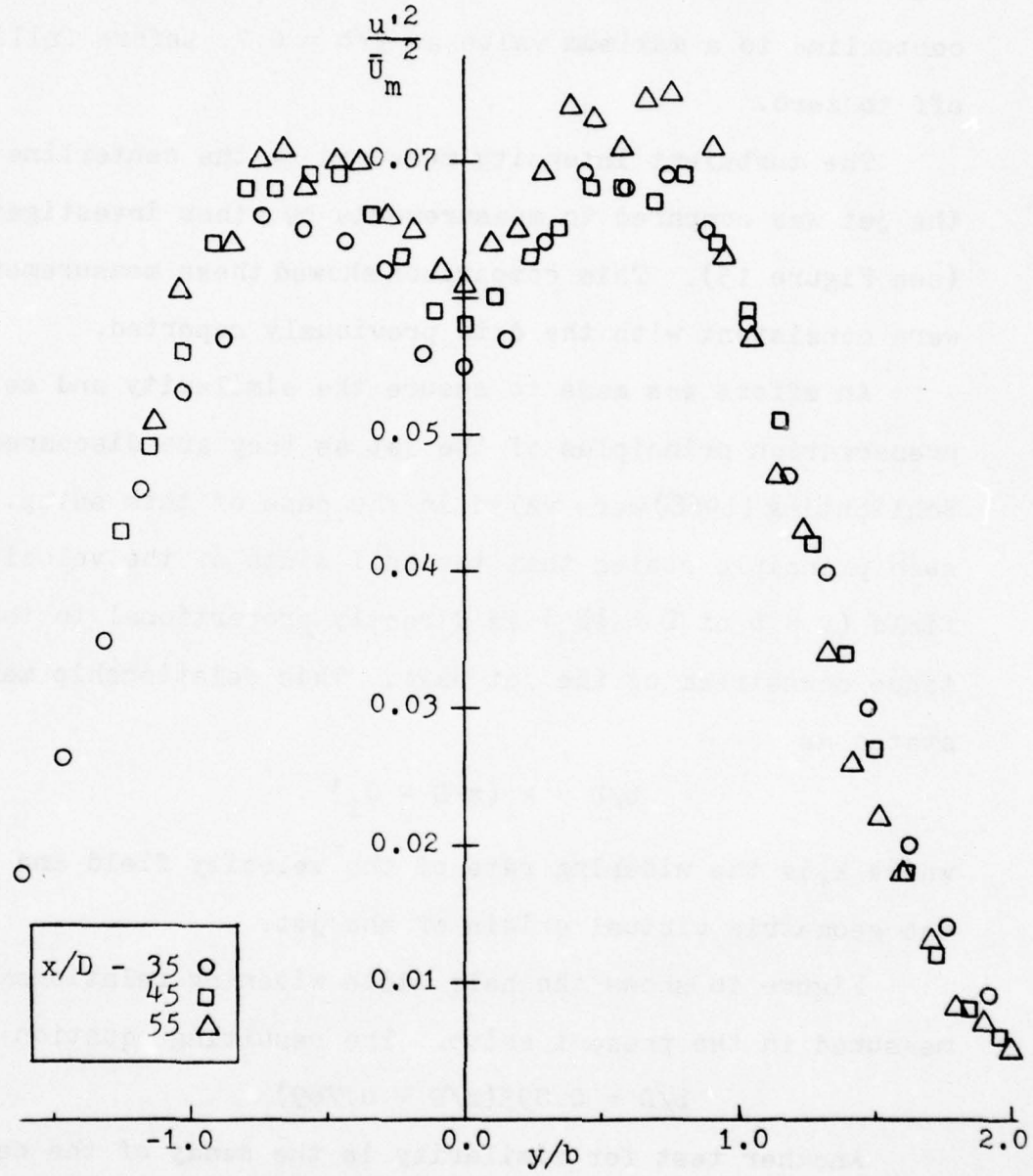

Figure 14 Turbulent Intensity Squared vs. y/b

The relative turbulent intensity showed agreement with previous work by other investigators. Bradbury (1965) showed a similar plot of turbulent intensity increasing from the centerline to a maximum value at $y/b = 0.7$, before falling off to zero.

The turbulent intensity measured at the centerline of the jet was compared to measurements by other investigators (see Figure 15). This comparison showed these measurements were consistent with the data previously reported.

An effort was made to assure the similarity and self-preservation principles of the jet as they are discussed by Schlichting (1968) were valid in the case of this setup. one such principle states that the half width of the velocity field ($y = b$ at $\bar{U} = \frac{1}{2}\bar{U}_m$) is directly proportional to the distance downstream of the jet exit. This relationship may be stated as

$$b/D = k_1(x/D - C_1)$$

where k_1 is the widening rate of the velocity field and C_1 is the geometric virtual origin of the jet.

Figure 16 shows the half width widening relationship as measured in the present setup. The resulting equation is

$$b/D = 0.095(x/D + 0.789) \qquad (9)$$

Another test for similarity is the decay of the centerline velocity. Theoretical considerations state the centerline velocity should be inversely proportional to the distance downstream of the jet exit squared. This relationship

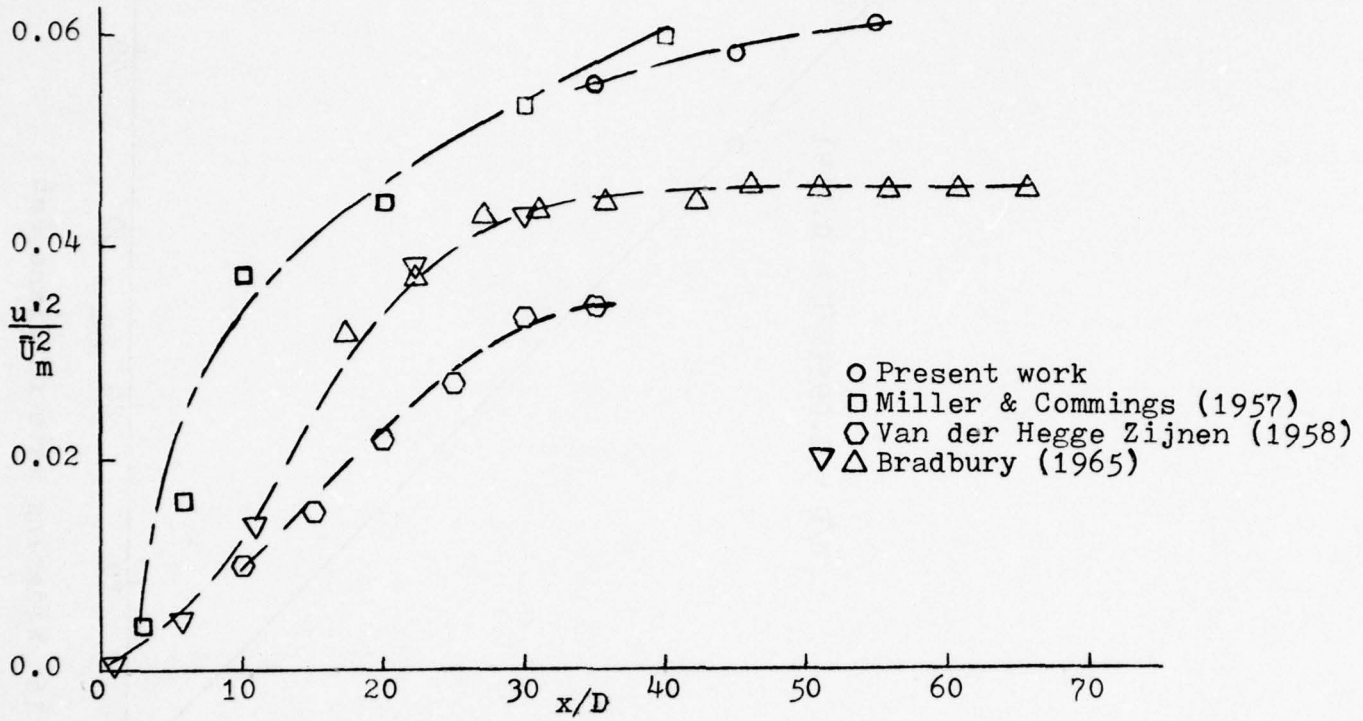

Figure 15 Variation of Turbulent Intensity Squared Along the Centerline of the Jet

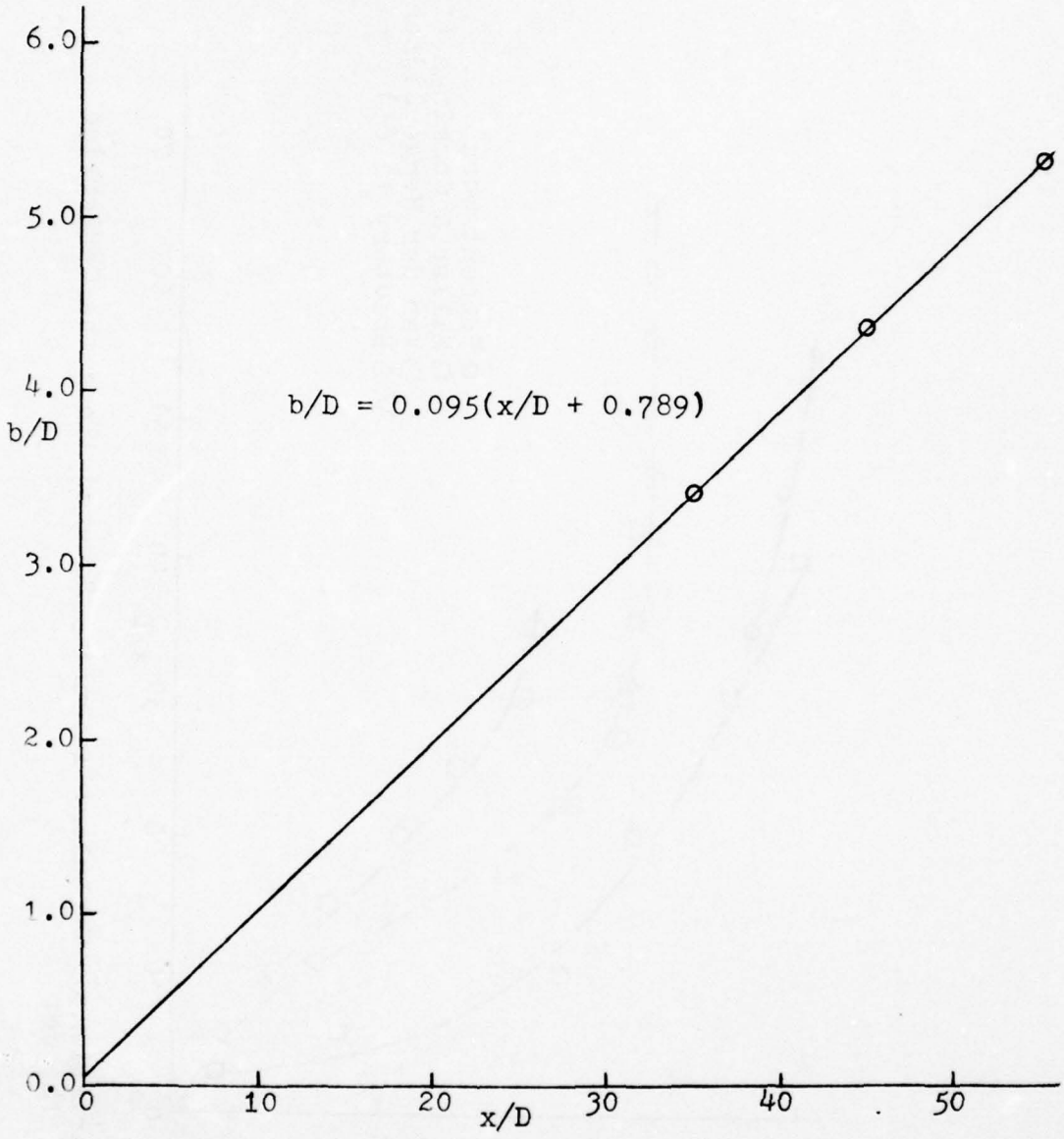

Figure 16 Widening Rate of Plane Jet

may be written in a linear form, as

$$\left(\frac{\bar{U}_m}{\bar{U}_o}\right)^{-2} = k_2(x/D - C_2)$$

where k_2 is the decay rate of the centerline velocity and C_2 is the kinematic virtual origin of the jet. As noted by Flora and Goldschmidt (1969), there is no reason to expect any relationship between the two virtual origins mentioned.

Figure 17 shows the parabolic decay of the centerline velocity. The empirical relationship is given as

$$\left(\frac{\bar{U}_m}{\bar{U}_o}\right)^{-2} = 0.185(x/D - 13.2) \qquad (10)$$

The empirical constants which were measured in this setup are compared with work by other investigators in Table 1. For Reynolds' numbers in a range of 1.0 to 8.0×10^4, the variation of the widening rate is 0.085–0.110 and of the decay rate of the centerline velocity is 0.150–0.364.

These results show that the experimental set up used for this work is in general agreement with previous investigators. Other tests, especially for the two dimensionality of the flow field have been reported previously by Jenkins (1974) and were not repeated by this author.

2. Procedure to Measure V_i

The procedure to measure the lateral velocity of the interface is described below. Figure 18 shows a schematic of the data measurement procedure. The output of the two

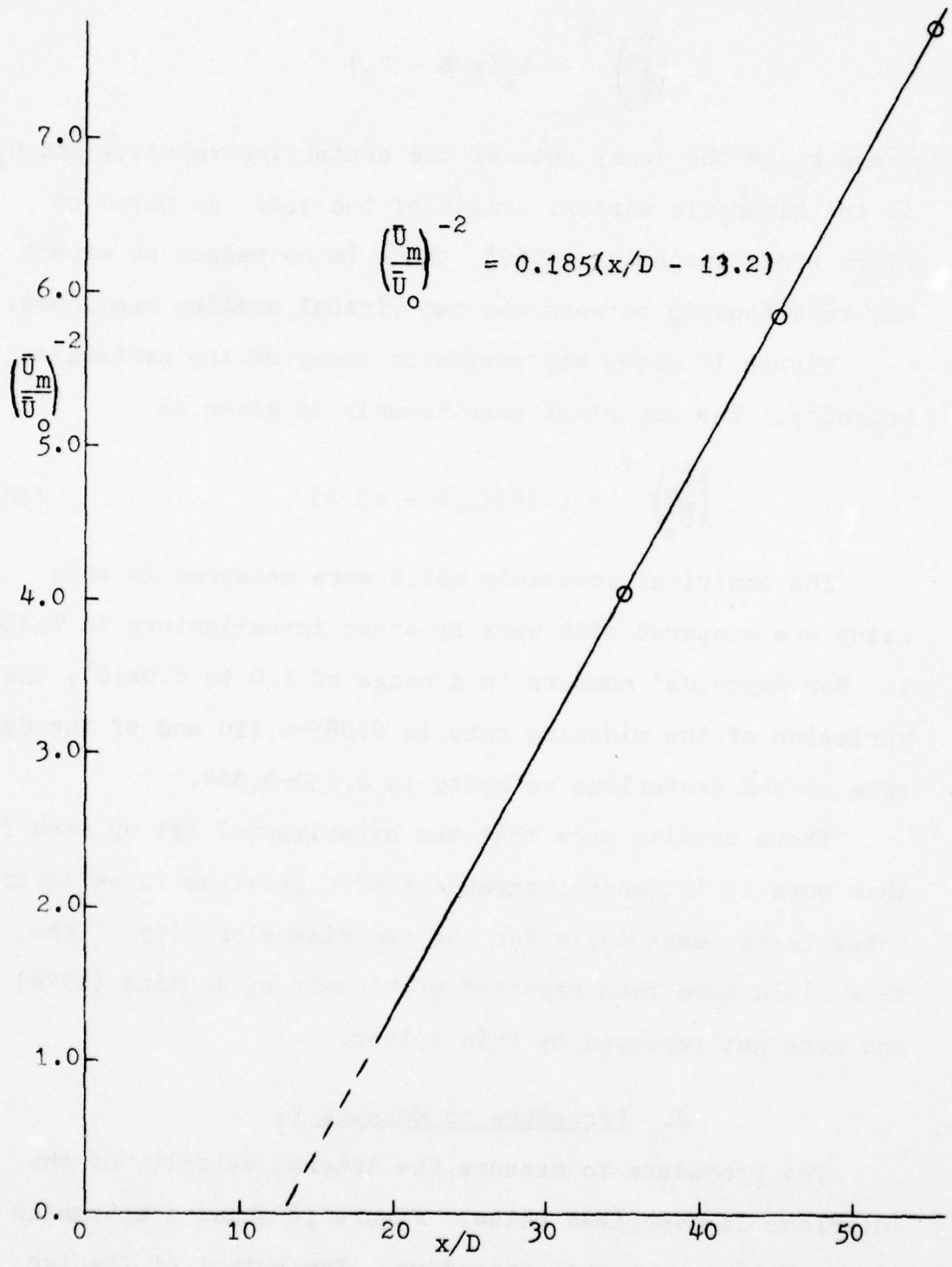

Figure 17 Centerline Velocity Decay Rate

Table 1 Characteristic Parameters of Plane Jets

Investigator	Re	k_1	k_2	C_1	C_2
Miller & Commings (1957)	1.78×10^4	0.0983	0.227	-1.572	-1.572
Van der Hegge Zijnen (1958)	1.33×10^4	0.100	0.205	0.0	-1.70
Foss (1965)	5.5×10^4	0.085	0.2565	-2.0	6.50
Heskestad (1965)*	2.5×10^4	0.110	0.364	5.3	5.3
Householder (1968)	$4.-8. \times 10^4$	0.0908	0.1927	-1.46	6.98
Flora (1969)	$2.-3. \times 10^4$	0.109–0.318	0.158–0.227	-15.0	2.0
Kaiser (1971)	$1.-4. \times 10^4$	0.101	0.208	-2.6	0.0
Ott (1972)	1.0×10^4	0.0968	0.228	-3.0	7.0
Young (1973)	1.0×10^4	0.0875	0.150	-8.75	-1.25
Jenkins (1974)**	1.45×10^4	0.091	0.160	-3.0	4.0
Present Work	1.6×10^4	0.095	0.185	-0.789	13.2

* mixing at the jet exit

** heated 20.7° above ambient

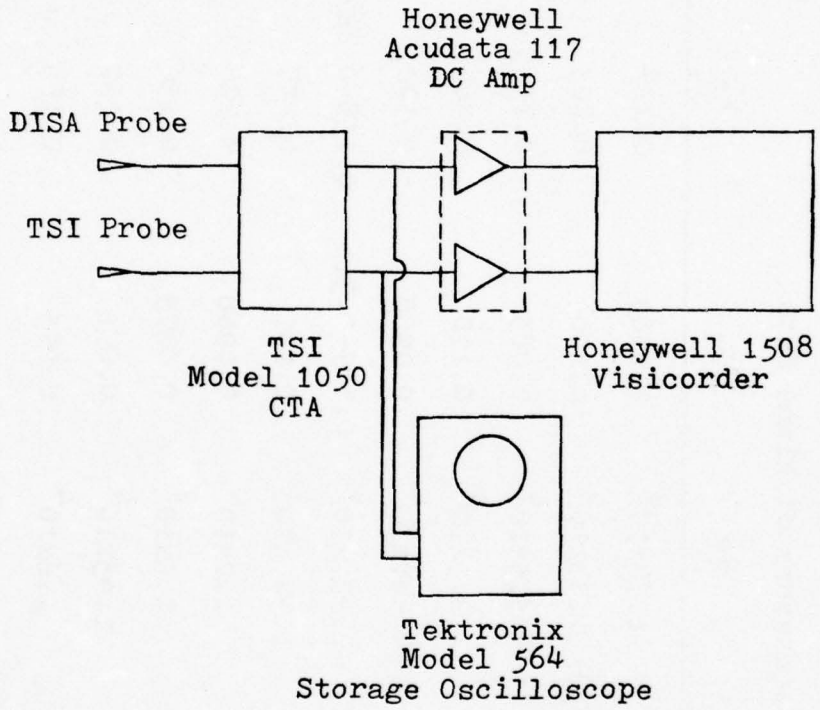

Figure 18 Schematic of Data Measurement Process

hot wire probes which are located in known positions in the flow field ((x_o,y_o) and $(x_o,y_o-\Delta y)$), are recorded simultaneously. Figure 2 shows a typical record on the visicorder which could also be monitored on the storage oscilloscope. Comparing the two simultaneous traces, the length of time it would take for the interface to travel between the two probes could be measured as the time, Δt, between the onset of turbulence from one probe to the onset of turbulence at the other probe. Averaging over sufficient values and knowing the separation of the two probes, Δy, the velocity of the interface as a function of the probe separation and the location in the jet may be determined as

$$V_i(x,y,\Delta y) = \frac{\Delta y}{\Delta t}$$

The positioning of the probes was done in the following manner. Probe 2 (see Figure 12) was positioned at the x/D station and y/b location of interest. The other probe (probe 3) was then positioned at different lateral separations, Δy, from the first probe[1]. Typically a minimum of three values of Δy were used to find $V_i(x,y,\Delta y)$. From them, the extrapolated V_i,

$$V_i(x,y) = \lim_{\Delta y \to 0} V_i(x,y,\Delta y)$$

was computed. This corresponds to the velocity of the interface at the point where probe 2 was located.

---

[1]Probes 2 and 3 mentioned here correspond to probes 2 and 1 respectively of Figure 1.

The presence of folding in the interface is a well established fact. Folding is encountered when a nonturbulent region or pocket of fluid exists closer to the jet axis than another turbulent region of fluid. One example of an interface configuration which would lead to folding is shown in Figure 19. The interface configuration is meant to correspond to the hot wire traces shown in the figure.

The occurrence of folding leads to difficulties in modeling the interface, as the interface can no longer be assumed to be single valued (see Paizis and Schwarz (1974)). The percentage of folding, ϕ_i, is a measure of the occurrence of folding in the interface. It is the fraction of total samples observed in which folding is noted, and is recognized to be a function of location in the flow field.

Another problem folding introduces is an ambiguity in the measure of the velocity of the interface. From Figure 19 the corresponding different values of V_i would be

$$V_{i1} = \Delta y/\tfrac{1}{4}(\Delta t_1 + \Delta t_4 + \Delta t_5 + \Delta t_6) \tag{11}$$

$$V_{i2} = \Delta y/\tfrac{1}{6}(\Delta t_1 + \Delta t_2 + \Delta t_3 + \Delta t_4 + \Delta t_5 + \Delta t_6) \tag{12}$$

$$V_{i3} = \Delta y/\tfrac{1}{6}(\Delta t_1 - \Delta t_2 - \Delta t_3 + \Delta t_4 + \Delta t_5 + \Delta t_6) \tag{13}$$

V_{i1} is a measure of the velocity of the interface neglecting the effects of folding. V_{i2} obtains a measure of the velocity of the interface considering the effects of the folding of the interface in magnitude only. V_{i3} considers both the direction and magnitude of the folding of the interface in

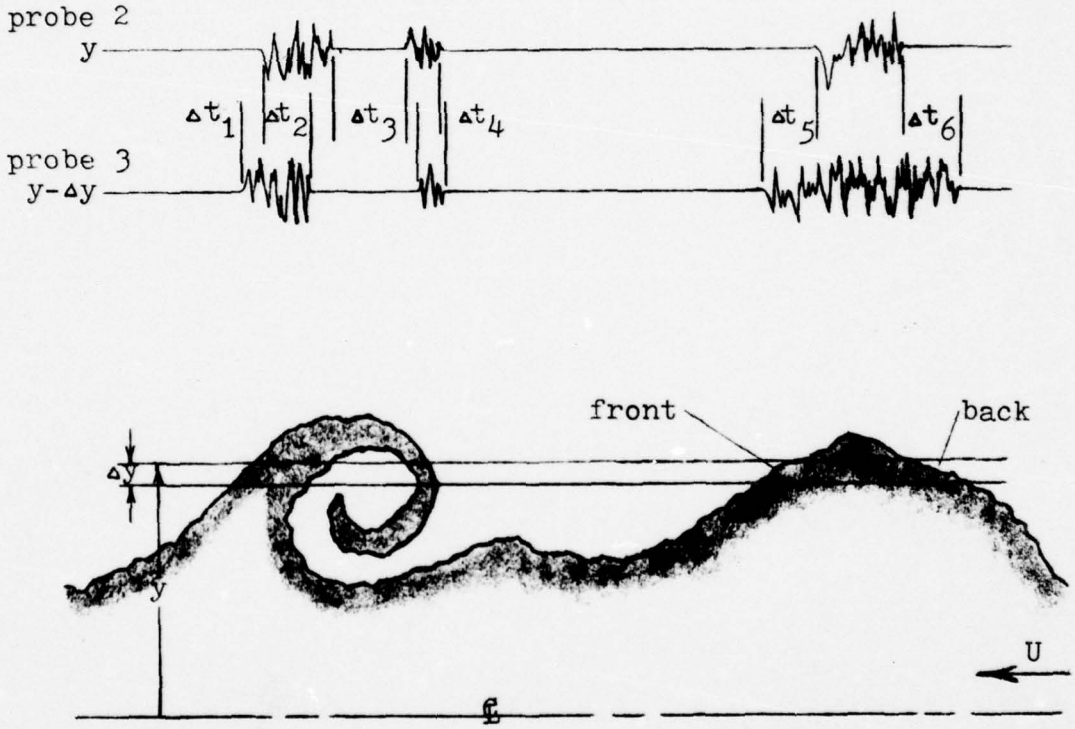

Figure 19 Possible Form of Interface With Output of Hot Wire Probes Showing Folding

its measure of the velocity of the interface. In the reported work, all three cases were considered although V_{i3} was chosen to be the most meaningful measure of the velocity of the interface.

III EXPERIMENTAL RESULTS

1. The Velocity of the Interface

The measurement of the velocity of the interface has been carried out as per the procedure given in the previous section. The results are shown and explained in this section.

Figure 20 shows the mean velocity of the interface, V_i, (specifically V_{i3} of Equation (13)) as a function of the lateral displacement in the plane jet for three different x/D stations. This figure shows a monotonic decrease of V_i as it moves away from the centerline of the jet (y/b=0). It should also be noted that no strong variation is seen with changes in axial location. This could be due to the limited range of x/D values or due to experimental scatter. In reality, similarity suggests that V_i should scale with U_m and/or $bf_{\gamma m}$.

There is some question as to the best method of nondimensionalizing V_i. Figures 21, 22 and 23 show V_i plotted in nondimensional terms. In the first plot, V_i is made nondimensional by b, the half width of the velocity field and $f_{\gamma m}$, the maximum crossing frequency. This grouping is suggested by the analysis used to predict the value of the velocity of the interface. The second plot shows V_i scaled by $\bar{U}_m$, the

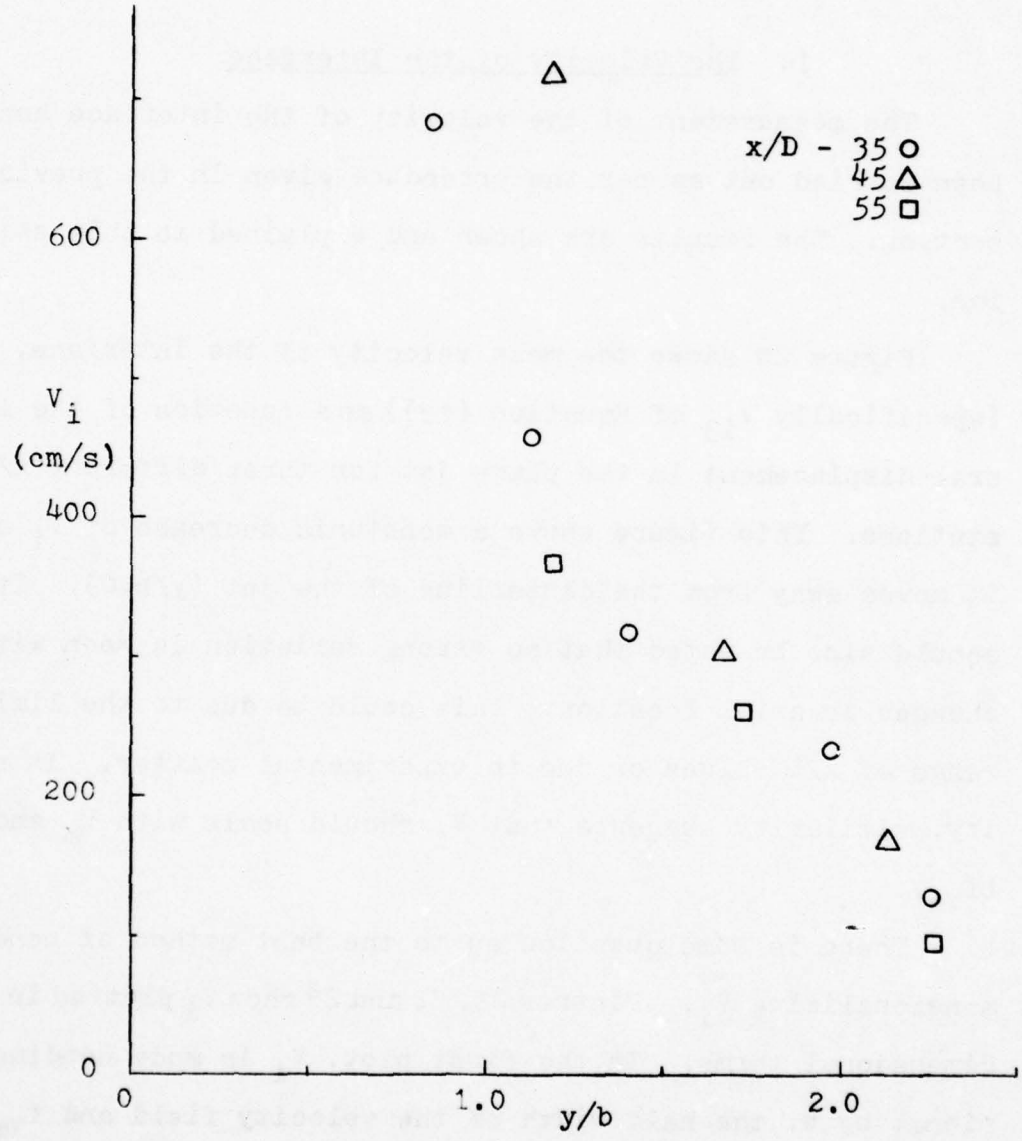

Figure 20 V_i vs. y/b

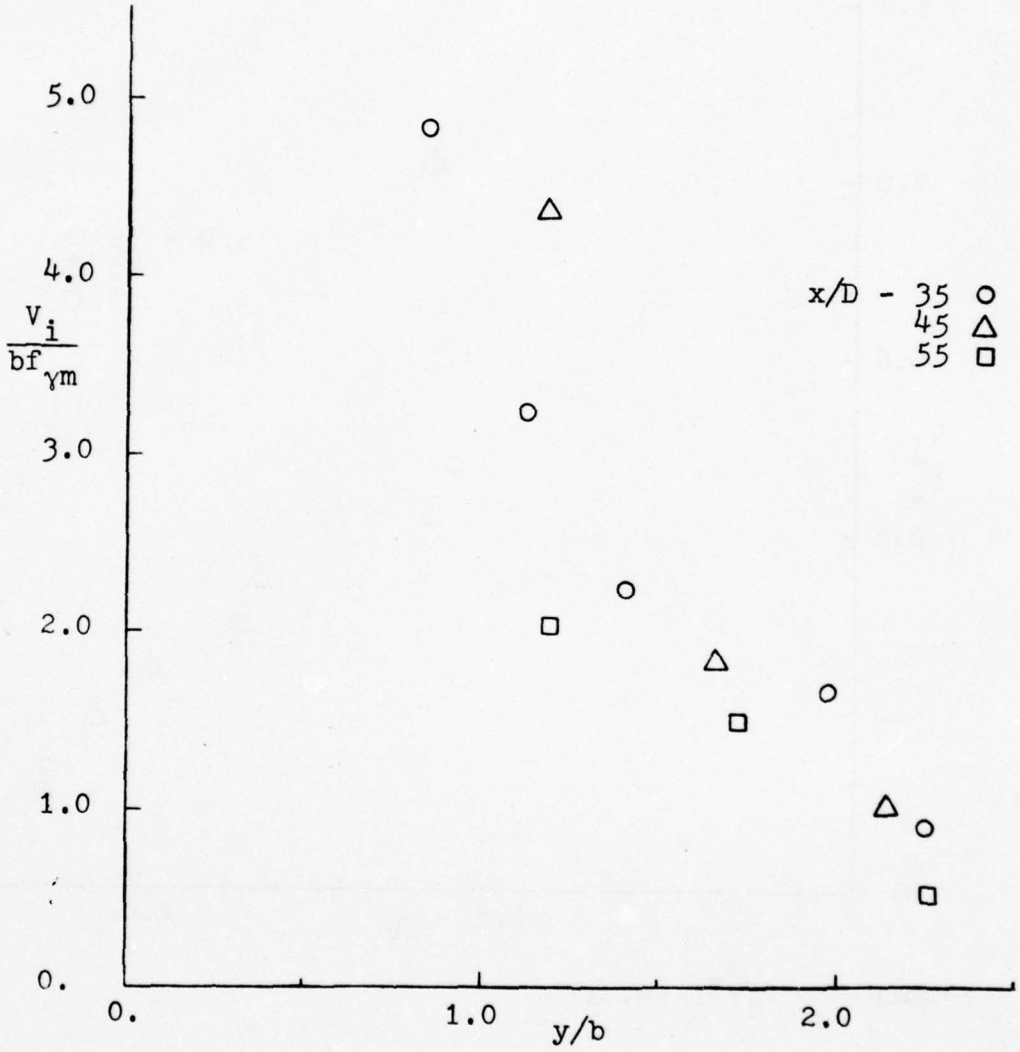

Figure 21 $V_i/bf_{\gamma m}$ vs.y/b

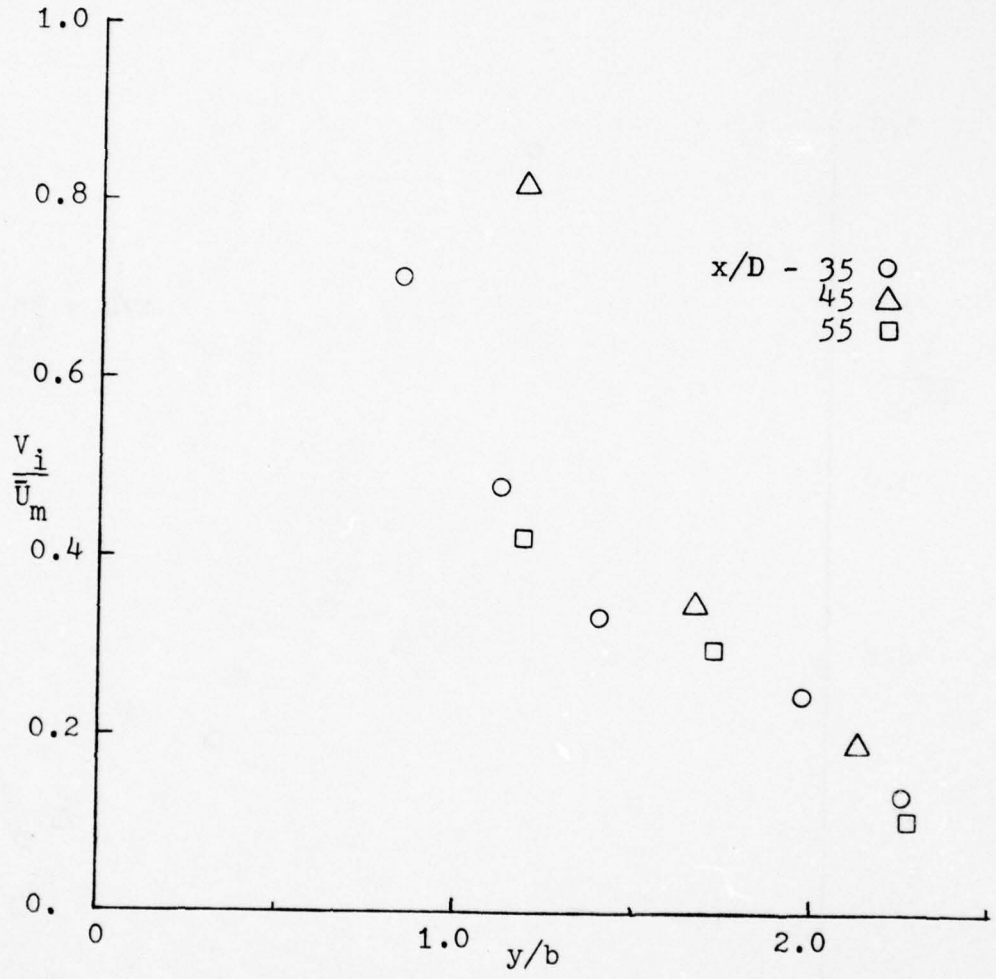

Figure 22 $V_i/\bar{U}_m$ vs. y/b

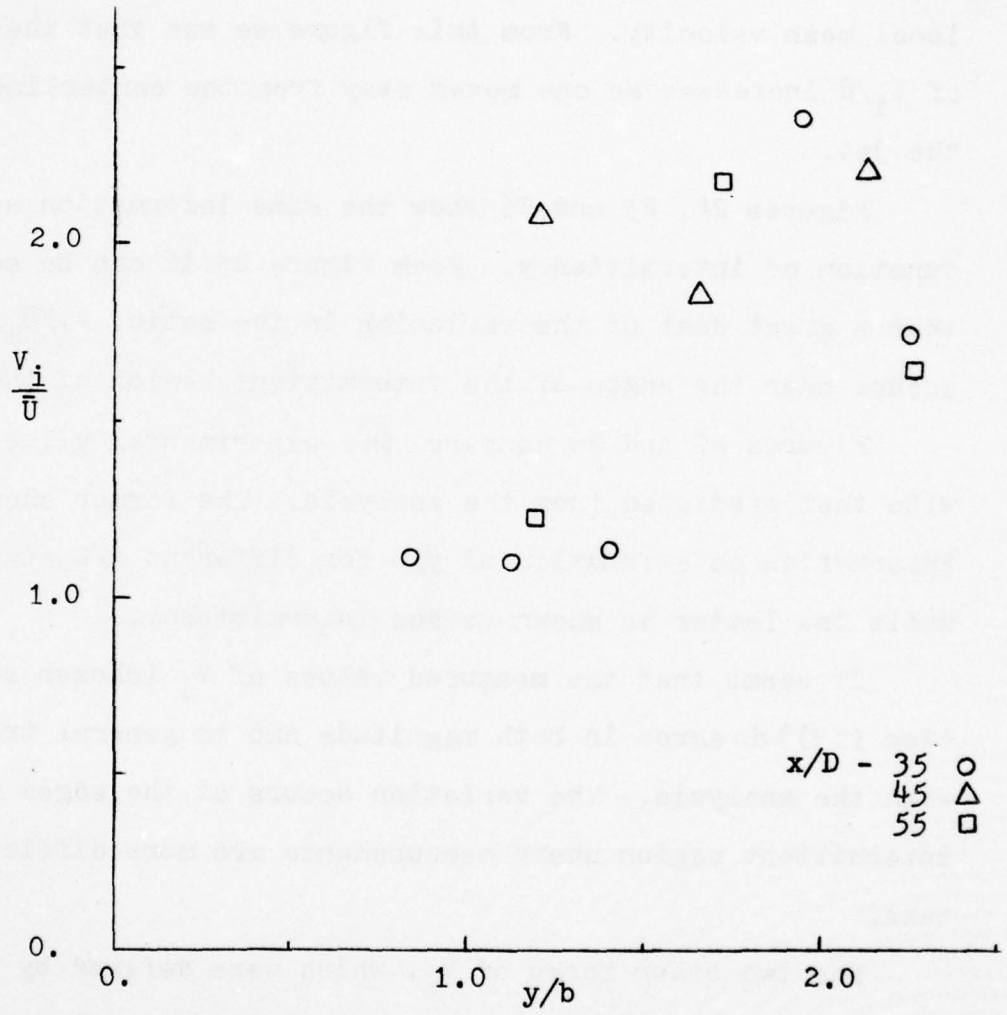

Figure 23 $V_i/\bar{U}$ vs. y/b

mean centerline velocity. This grouping seems to give a reasonable scaling of the data. It shows the order of magnitude of V_i to range from 0.8 to 0.1 of the mean centerline velocity while moving through the intermittent region of the jet. The third plot shows V_i made nondimensional by $\bar{U}$, the local mean velocity. From this figure we see that the ratio of $V_i/\bar{U}$ increases as one moves away from the centerline of the jet.

Figures 24, 25 and 26 show the same information as a function of intermittency. From Figure 25 it can be seen that a great deal of the variation in the ratio, $V_i/\bar{U}_m$, occurs near the edges of the intermittent region of the jet.

Figures 27 and 28 compare the experimental values of V_i with that predicted from the analysis. The former shows the information as a function of y/b for different x/D stations, while the latter is shown versus intermittency.

It seems that the measured values of V_i (chosen as Equation (13)) do agree in both magnitude and in general trend with the analysis. The variation occurs at the edges of the intermittent region where measurements are more difficult to take.

The two other forms of V_i, which were defined by Equations (11) and (12) and required due to the existence of foldover, are compared with the values predicted from the analysis in Figures 29 and 30. Figure 29 shows V_{i1} in nondimensional terms compared with the predicted value of V_i. V_{i1} may be thought of as the velocity of the interface

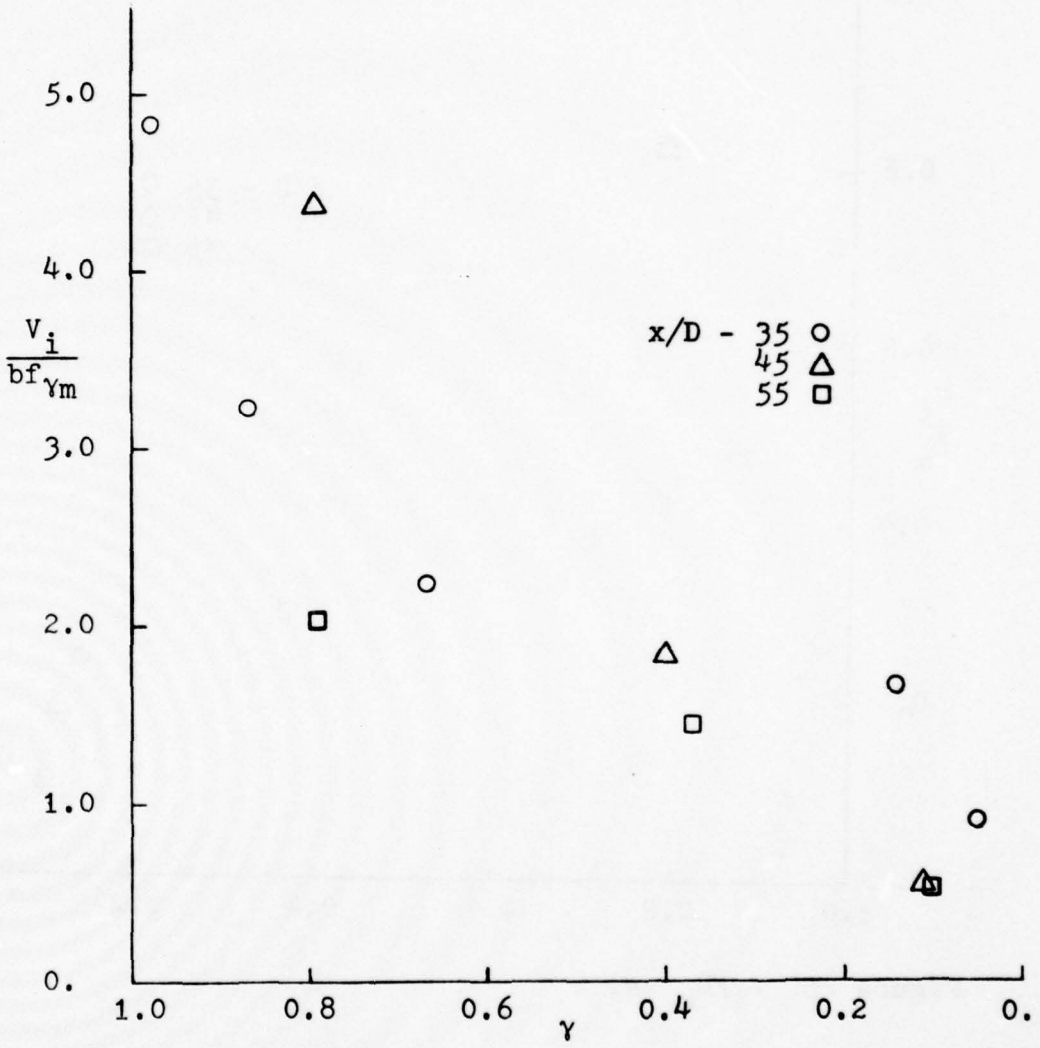

Figure 24 $V_i/bf_{\gamma m}$ vs. γ

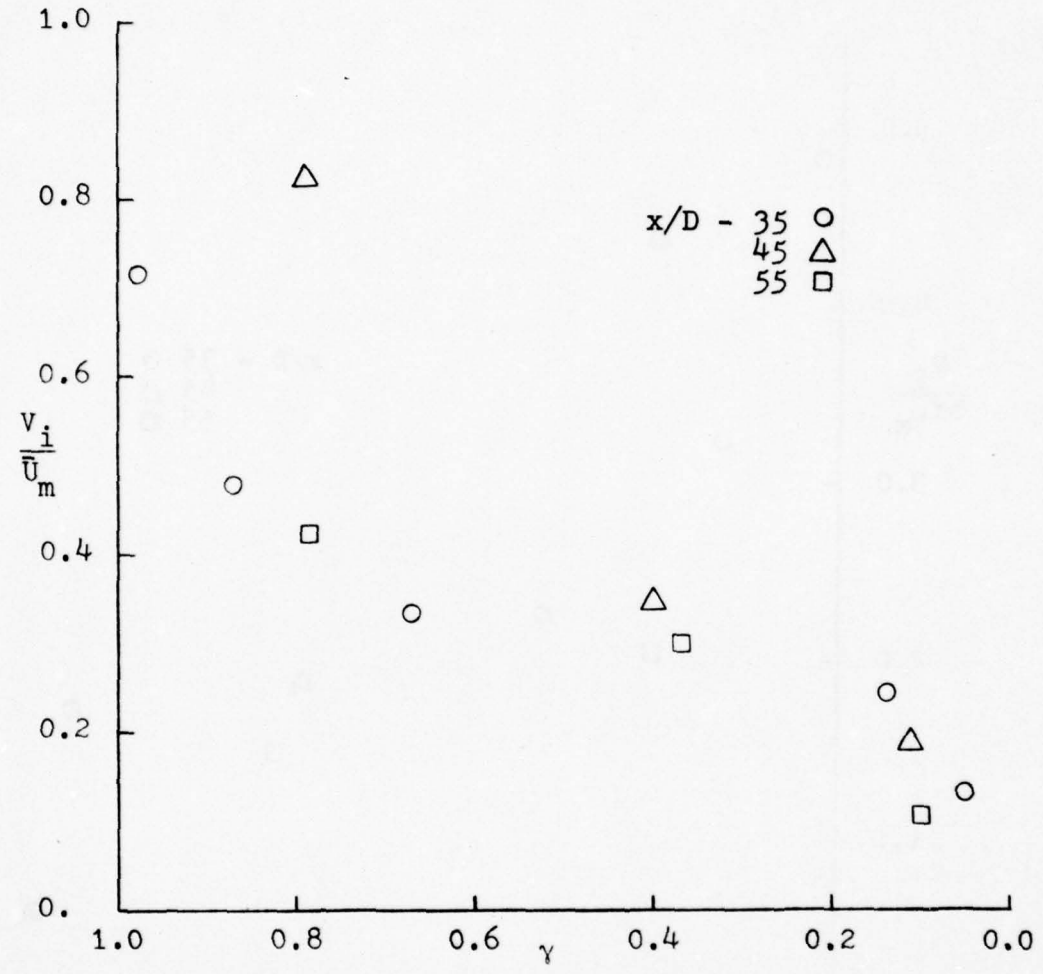

Figure 25 $V_i/\bar{U}_m$ vs. γ

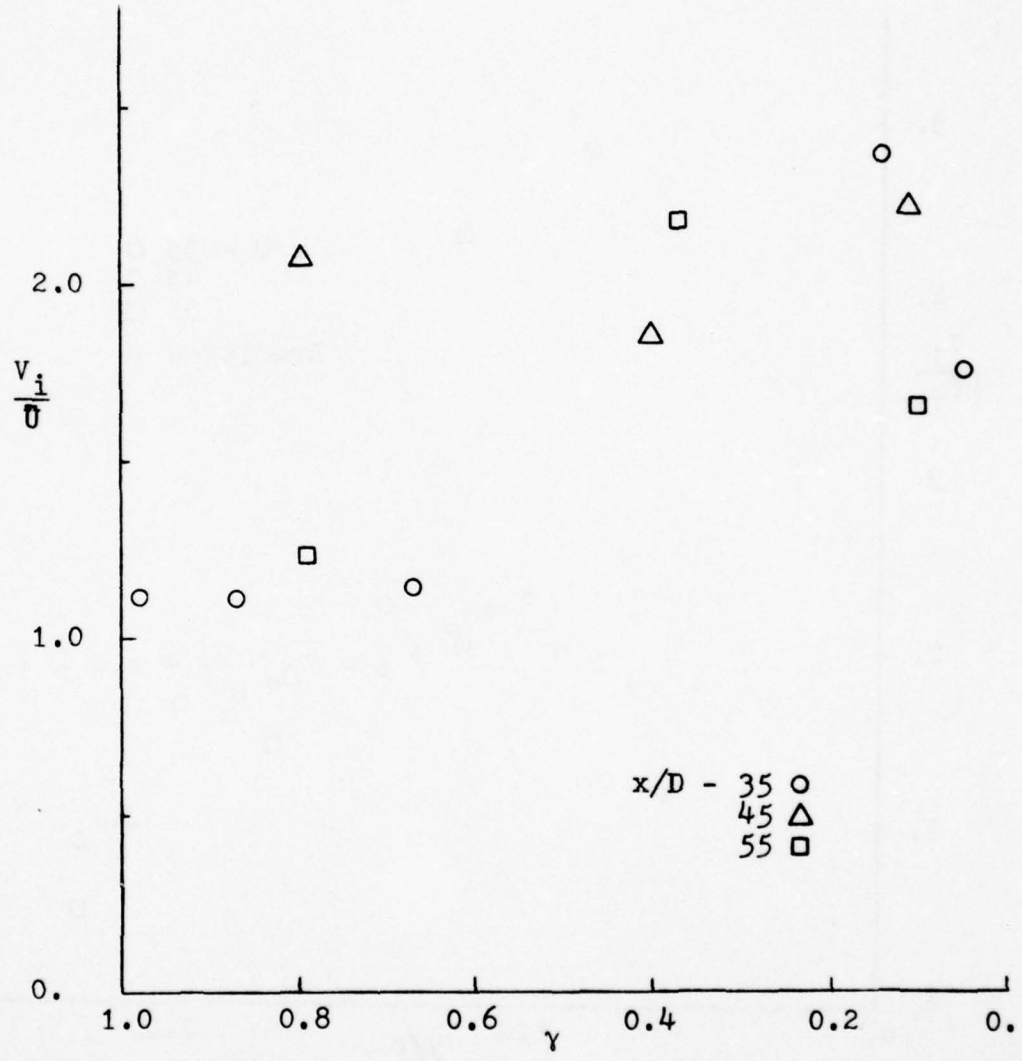

Figure 26 $V_i/\bar{U}$ vs. γ

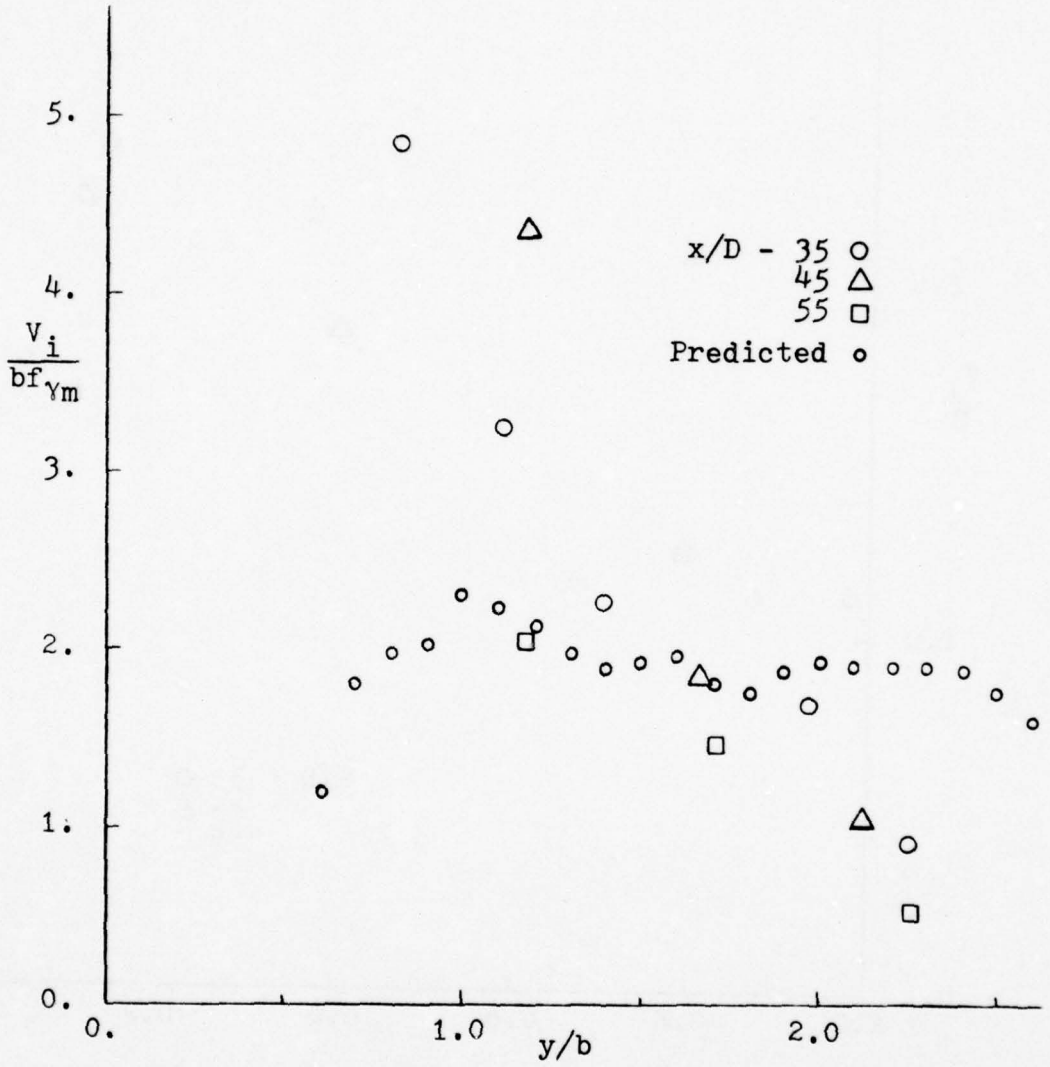

Figure 27 Comparison of V_i with Predicted Value vs. y/b

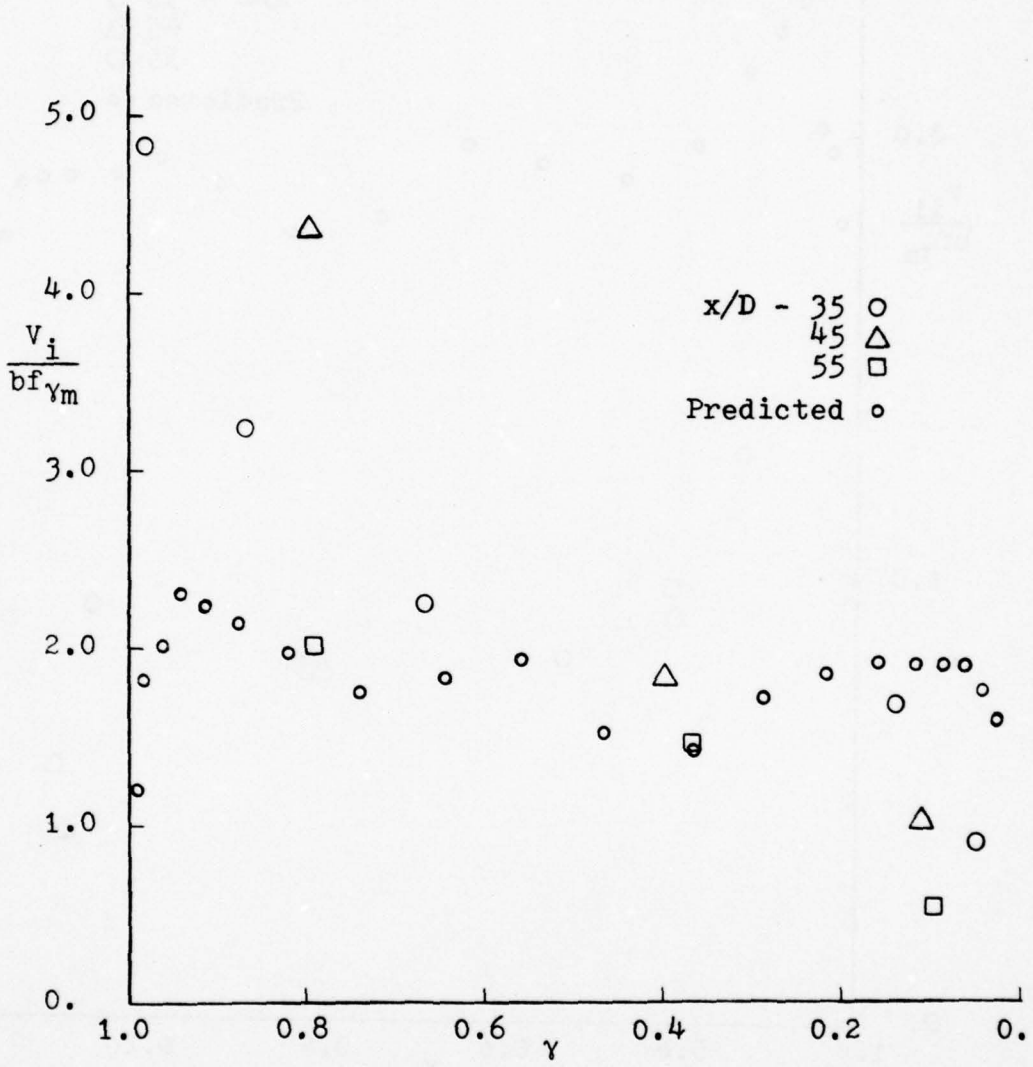

Figure 28 Comparison of V_i with Predicted Value vs. γ

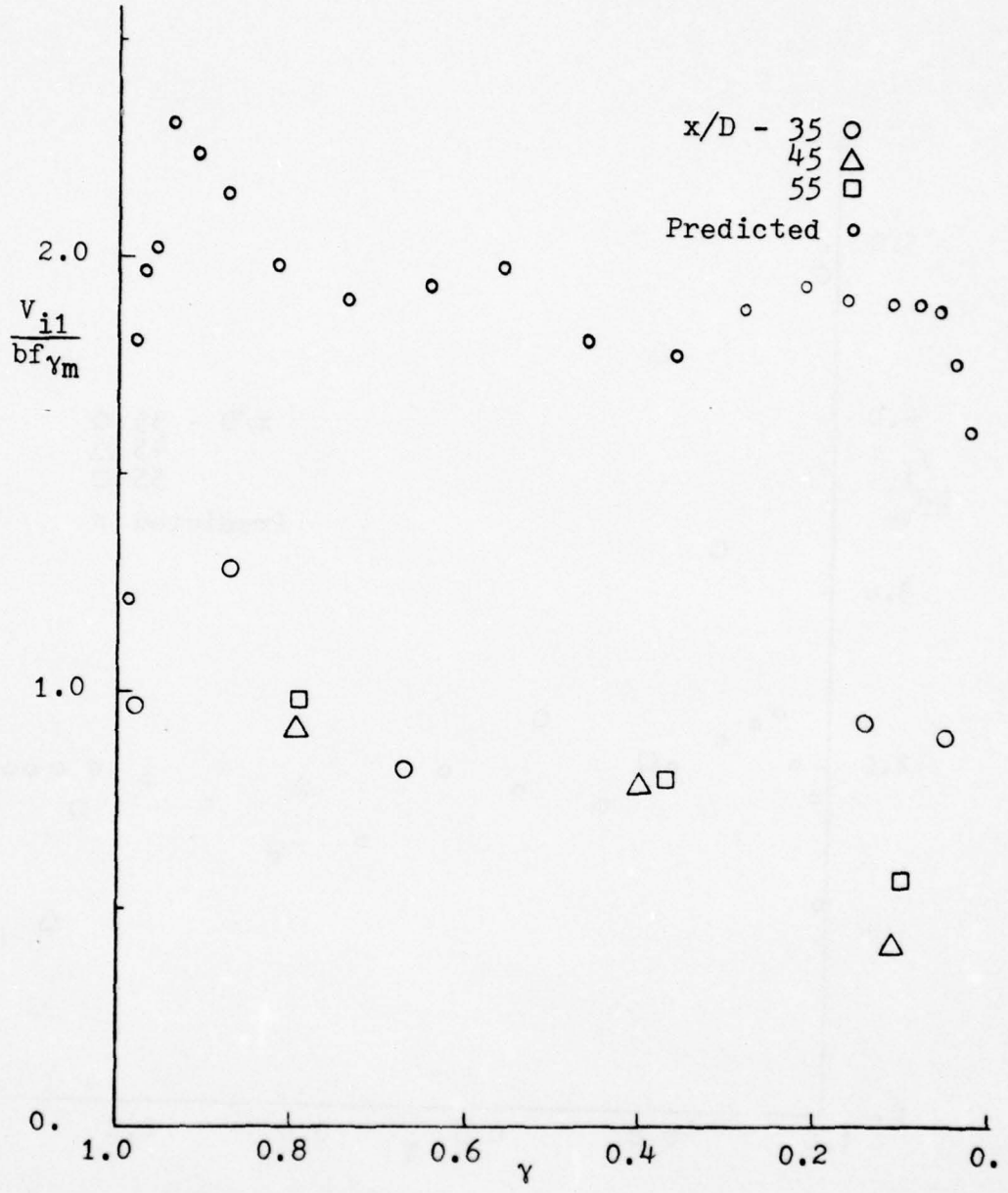

Figure 29 Comparison of V_{i1} with Predicted Value vs. γ

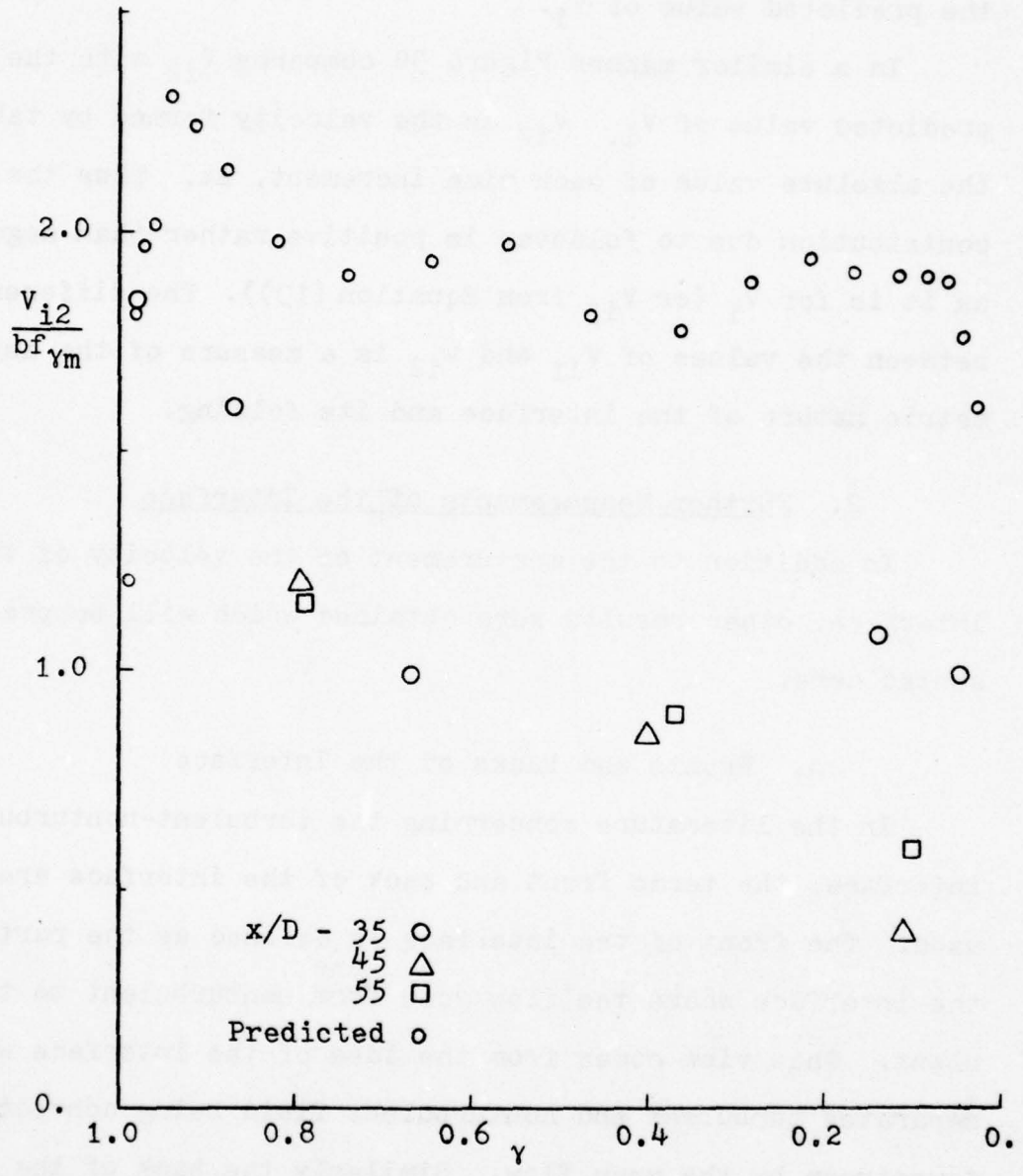

Figure 30 Comparison of V_{i2} with Predicted Value vs. γ

without considering the folding of the interface. As shown in Figure 29, the measured value of V_{i1} appears to be half the predicted value of V_i.

In a similar manner Figure 30 compares V_{i2} with the predicted value of V_i. V_{i2} is the velocity formed by taking the absolute value of each time increment, Δt. Thus the contribution due to foldover is positive rather than negative as it is for V_i (or V_{i3} from Equation (13)). The difference between the values of V_{i1} and V_{i2} is a measure of the asymmetric nature of the interface and its folding.

2. Further Measurements of the Interface

In addition to the measurement of the velocity of the interface, other results were obtained which will be presented here.

a. Fronts and Backs of the Interface

In the literature concerning the turbulent-nonturbulent interface, the terms front and back of the interface are used. The front of the interface is defined as the part of the interface where the flow goes from nonturbulent to turbulent. This view comes from the idea of the interface which separates turbulent and nonturbulent fluid being convected downstream by the mean flow. Similarly the back of the interface is the part where the flow goes from turbulent to nonturbulent fluid. This may be seen in Figure 19 which shows a possible shape of the interface.

If the model of the interface is taken as that of the interface moving laterally in a varying periodic motion, then the front of the interface would correspond to the part of the interface indicated by the time increments Δt_1 and Δt_5 in Figure 19. This is an apparent outward motion (away from the jet centerline) of the interface. In a similar manner, the back of the interface would correspond to the time increments Δt_4 and Δt_6 of Figure 19 and could be interpreted as an inward motion of the interface.

The point of discussion is that the fronts and backs of the interface are not necessarily identical (symmetric). Paizis and Schwarz (1974) discuss this for their work in a wall jet and have found that the slope of the front of the interface is steeper than the slope on the back of the interface. Oswald and Kibens (1971) have also found the fronts and backs of the turbulent-nonturbulent interface to differ in the wake of a circular disk. They have taken measurements which show that the convective velocity of the front of the interface is faster than the convective velocity of the back. Figure 31 compares the velocity of the front of the interface with the velocity of the back. This shows that the interface appears to move outward faster than it moves inward. This could be a result of the difference in the slopes of the front and back of the interface which is discussed in the work of Paizis and Schwarz (1974).

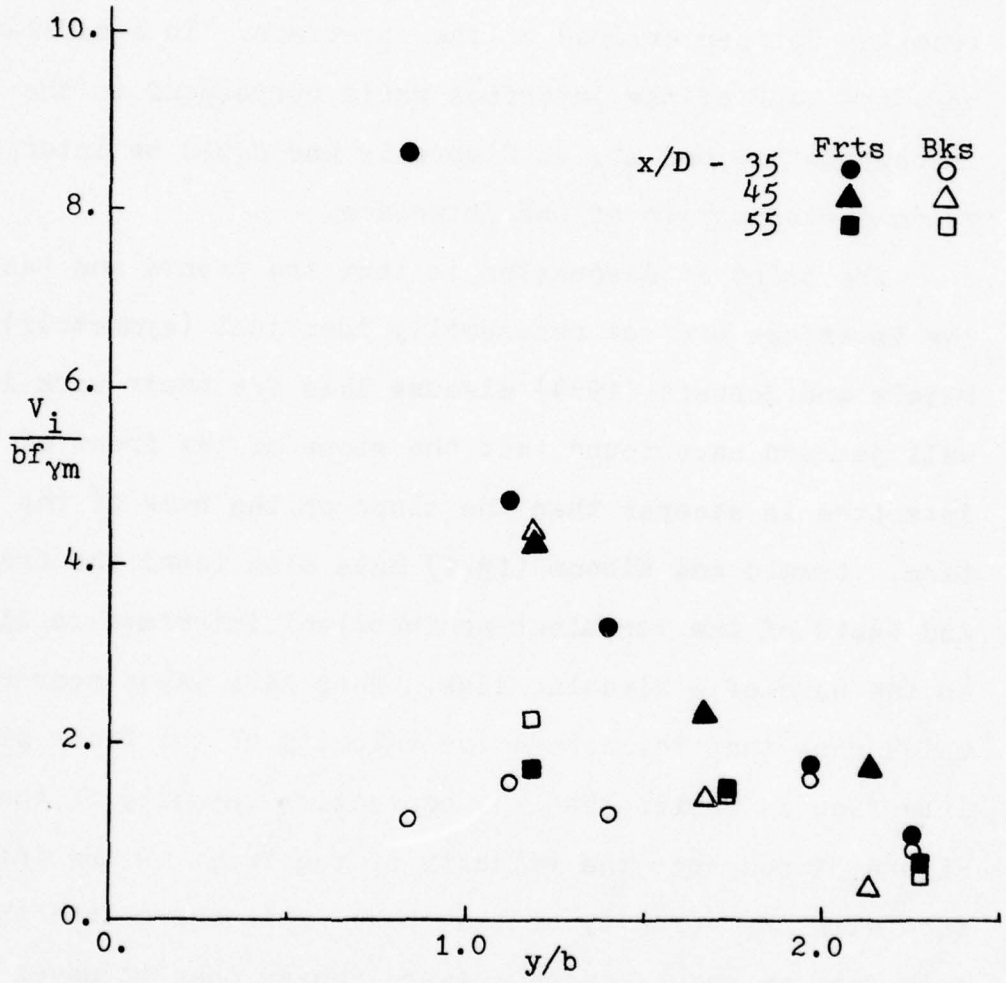

Figure 31 Velocity of the Fronts and Backs of the Interface vs. y/b

b. Folding

The possible presence of folding in the interface has been a source of uncertainty in conditional measurements. Its presence in the case of a wall jet was first noted by Paizis and Schwarz (1974), although ambiguity in the gate level of their turbulence detectors could have lead to the apparent presence of folding. In this work the observation of simultaneous traces such as shown in Figure 2 has convincingly indicated the presence of folding (as per the schematic of Figure 19).

The parameter, ϕ_i, was defined as the percentage of folding in the interface. ϕ_i is shown in Figure 32 as a function of the location in the jet. ϕ_i is also shown in Figure 33 for both the front and back of the interface as a function of location in the jet. From these two figures it seems that folding is more likely to occur toward the centerline of the jet (in the intermittent region) and more likely to be detected on the front of the interface. It should be noted that there can be no folding outside the intermittent region.

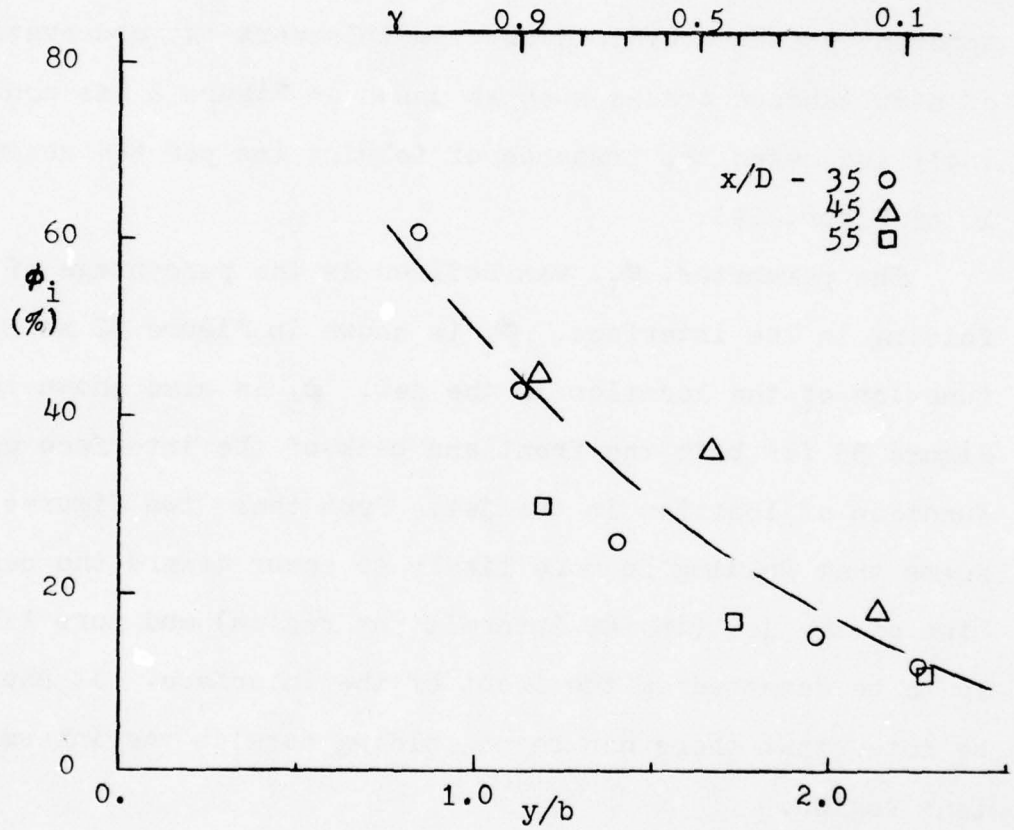

Figure 32 Percentage Folding vs. y/b

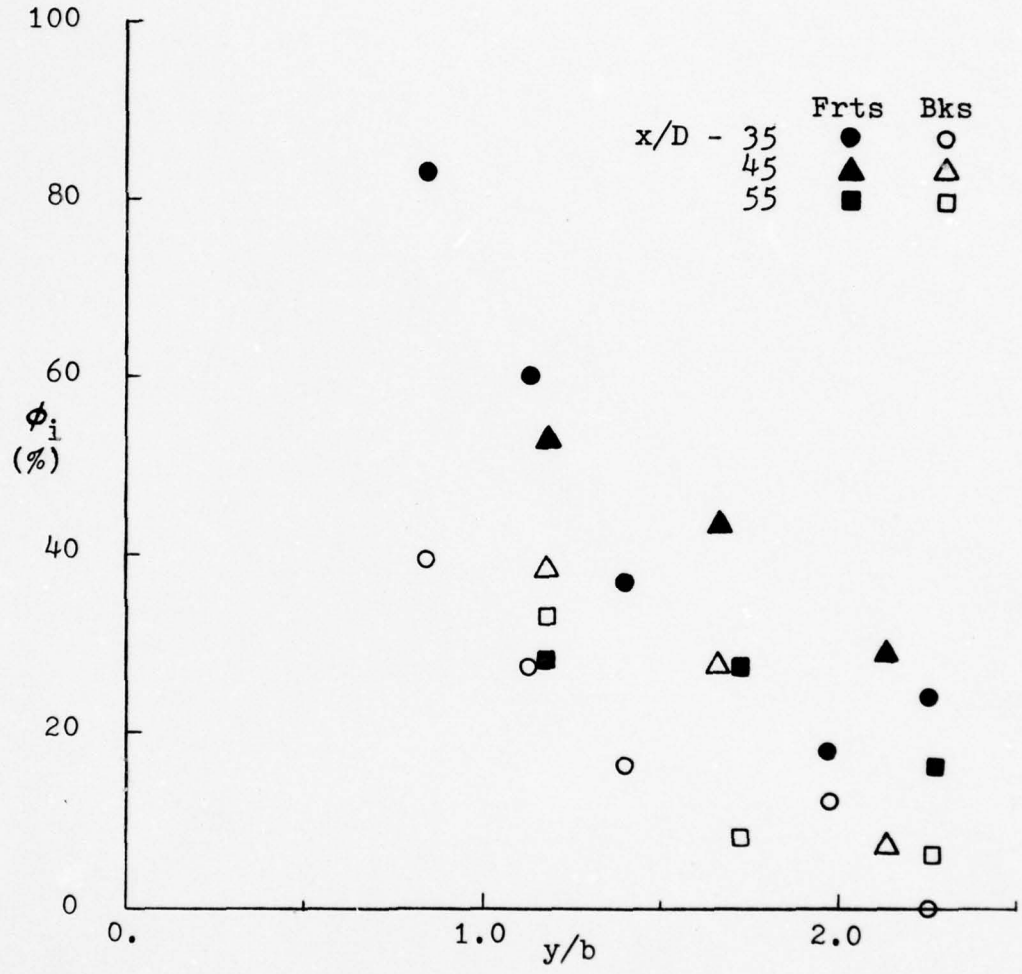

Figure 33 Percentage Folding for Fronts and Backs of the Interface vs. y/b

IV DISCUSSION OF RESULTS

This work has been mostly experimental with the emphasis placed on measurements taken in the laboratory. However there is one analytical result which has come from this work and deserves to be mentioned here. The expression for the velocity of the interface,

$$V_i = \frac{-2f_\gamma}{\partial\gamma/\partial y} \tag{6}$$

which was derived in Chapter II from basic parameters of turbulent flows was compared for different shear flows. There was a trend of similarity noted for the flows analyzed. This is significant in that this is the first time a characteristic velocity of the interface has been identified showing similarity for different situations.

1. Experimental Accuracy

In order to quantify the accuracy of the measurements reported, an analysis of the experimental accuracy of the measurements will be presented.

Applying an uncertainty analysis to V_i or $V_i(\Delta y)$, the primary measured quantity, an estimate of the uncertainty may be obtained (Appendix C shows the method used to obtain V_i from the data taken from the visicorder traces): the

source of error in the measurements to obtain $V_i(\Delta y)$ comes from uncertainty in the measure of Δt from the visicorder charts and Δy, the probe separation. For example, the uncertainty in $V_i(\Delta y=0.254)$ based on a single measure of Δt would be ± 37.2% (this is the sum of $\delta\Delta t/\Delta t$ = ±29.3% and $\delta\Delta y/\Delta y$ = ±7.9%). If all the time increments, Δt, were of the same duration, the uncertainty due to the measure of Δt would be reduced by a factor of the inverse of the square root of the number of samples taken. Using this factor the uncertainty of $V_i(\Delta y=0.254)$ is reduced to ±12.2% and the uncertainty of $V_i(x,y)$ found by extrapolation is ±13.5%.

The fact is that the time increments are not all of the same duration. Hence, in order to obtain a meaningful average, a large number of samples must be recorded. The actual number of samples recorded was limited by two constraints. One the laborious manual process employed in collecting the samples, and secondly their distribution due to the physical location of the probes in the intermittent region.

If it is assumed that the measured values of Δt follow a normal distribution, then an estimate of the further error in $V_i(x,y)$ due to the number of samples taken to obtain the mean value can be obtained.

Data was taken at eleven points throughout the fully developed region of the jet and at a total of 36 settings of $(x,y,\Delta y)$. The mean number of samples of the time increment, Δt, taken at each setting was 38 with a range of 12 to 74 samples. The number of samples taken was dependent primarily

on two factors: the y/b location in the jet and the probe separation. The determination of Δt from the visicorder traces was difficult for large probe separations and at the edges of the intermittent region ($\gamma \cong 0.0$ or $\gamma \cong 1.0$). It should be noted that at the smallest probe separations the number of samples was consistently large.

In an effort to determine how the number of samples affected the accuracy of $\overline{\Delta t}$ (and hence, $V_i(x,y)$), the standard deviation of the mean, σ_m, given as

$$\sigma_m = \frac{\sigma}{\sqrt{n}}$$

was calculated. σ is the standard deviation of the set of samples measured and n is the number of samples in the set. For a typical case the ratio $\sigma_m/\overline{\Delta t}$ was found to be 0.3. This then implies a standard deviation of the mean value of $V_i(\Delta y)$ due to the number of samples taken to be ±30% and a corresponding probable error of about 20%. This error is in addition to the uncertainty calculated above.

From this analysis the measurements of $V_i(x,y)$ taken and reported in this work show an uncertainty of ±13.5% due to the measurement procedure and a probable error of ±20% due to the number of samples taken. This would give an error band of ±33% about the measured values of $V_i(x,y)$. This seems quite reasonable for the type of measurement taken.

2. <u>The Asymmetric Nature of the Interface</u>

One characteristic of the interface which has been brought forth by this work is its lack of symmetry. This was

mentioned previously when V_{i1}, V_{i2}, and V_{i3} were introduced (see Equations (11), (12), and (13) and Figures 28 through 30). The difference between V_{i3} and V_{i1} is expected since V_{i3} accounts for the negative components of Δt which V_{i1} neglects. However the difference between V_{i2} and V_{i1} might not be expected since V_{i2} is simply the magnitude of the velocity without regard to direction. If the magnitude of Δt due to folding was the same as the normal values of Δt, then V_{i2} would be the same as V_{i1}. This is not the case as can be seen from a comparison of Figures 29 and 30. This shows that the velocity of the interface during folding is different than that without folding.

Another aspect of the asymmetric nature of the interface is the marked difference between the velocities of the front and back of the interface. Paizis and Schwarz (1974) in their work in a turbulent wall jet, noted that the slope of the front of the interface ($\partial y_i/\partial x$) was greater than the slope of the back of the interface. This is in agreement with this current work. The velocities of the interface for the front and back of the interface (see Figure 31) may be related to the slope of the interface by the relationship

$$\frac{\partial y_i}{\partial x} = \frac{\partial y_i/\partial t}{\partial x/\partial t} \quad \frac{V_i}{U}$$

This has been done for $x/D = 35$ and is shown in Figure 34. The figure clearly shows the difference between the front and back of the interface when considering an average shape including all folding and non-folding cases.

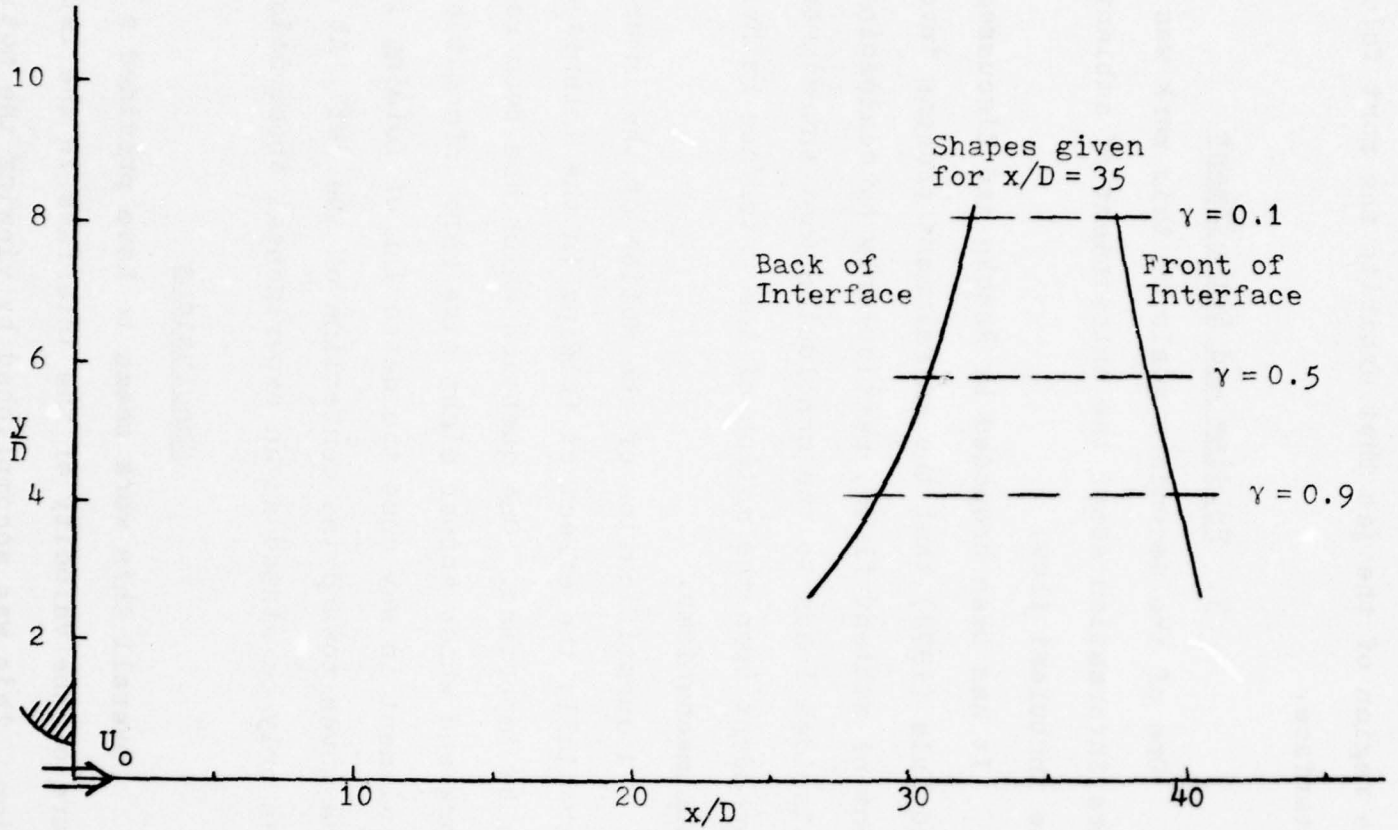

Figure 34. Average Shape of the Interface

Most of the difference occurs at $\gamma \geq 0.5$ which coincides with the region of the jet that exhibits the most folding in the interface.

3. Folding and Entrainment

One of the secondary goals of this work was to provide more information about the entrainment of ambient fluid into the turbulent flow.

It has been proposed by Roshko and discussed by Davies and Yule (1974) that the entrainment process involves engulfment of ambient fluid, particularly by coalescing eddies. This idea leads to the conclusion that entrainment would be dependent upon the motion of the interface rather than viscous mechanisms.

A quantification of the motion of the interface and especially the effect of folding in the interface would seem to be important. One question which has been raised by this work and whose answer might give more information about entrainment is why does the detection of folding increase as one moves toward the centerline of the jet? At present this can only be stated as an experimental observation.

Conclusions

Overall this work seems to have provided a unique measure of the velocity of the interface in the lateral direction. This was accomplished by viewing the motion of the interface in a manner different from earlier investigators. Other characteristics of the interface have also been

measured in a two dimensional plane jet for the first time. These characteristics, especially the detection of folding in the interface, may lead to a method of understanding entrainment in turbulent shear flows.

V FUTURE WORK

It was felt that there should be some discussion of the future work to be undertaken as a continuation of this current work. There are two areas which it is felt are of interest and will be investigated in the future.

The first area is the interface and its characteristics. There has been no real attempt made here to model the interface, although the view of the interface given by V_i may lead naturally to a model. There is also a need to apply some model to the problem of entrainment. This should be one of the goals in any future work in addition to more experimental measurements of the interface.

The second area of interest is concerned with conditional averaged measurements in a two dimensional plane jet. As an extension of the work by Jenkins (1974), the intention is to take measurements of the lateral scales of turbulence in the fully turbulent region. The result is a measure of the scales with respect to the interface at different locations in the jet.

The purpose of these latter measurements is to shed some insight on free shear flows and answer the question—how does shear change the turbulent structure within the turbulent region itself? Appendix B contains more information on these measurements.

LIST OF REFERENCES

1. Bradbury, L. J. S., "The Structure of a Self-Preserving Turbulent Plane Jet," J. Fluid Mech. Vol 23, Part 1, pp. 31-64, 1965.

2. Bradshaw, P., "Irrotational Fluctuations Near A Turbulent Boundary Layer," J. Fluid Mech. Vol. 27, Part 2, pp. 209-230, 1967.

3.1 Corrsin, S., "Investigation of Flow in an Axially Symmetrical Heated Jet of Air," NACA ACR No. 3623, 1943.

4. Corrsin, S. and Kistler, A. L., "The Free Stream Boundaries of Turbulent Flows," NACA TN 3133, 1954.

5. Davies, P. O. A. L. and Yule, A. J., "Coherent Structures in Turbulence," Proceedings of Colloquium on Coherent Structures in Turbulence, Southampton, March, 1974.

6. Flora, J. J. and Goldschmidt, V. W., "Virtual Origins of a Free Plane Turbulent Jet," AIAA Journal Vol. 7, No. 12, pp. 2344-2346, December, 1969.

7. Foss, J. F., "A Study of Incompressible Bounded Turbulent Jets," Ph. D. Thesis, Purdue University, January, 1965.

8. Heskestad, G., "Hot Wire Measurements in a Plane Turbulent Jet," Trans. of ASME Journal of Appld. Mech. Vol. 32, No. 4, pp. 221-234, December, 1965.

9. Hinze, J. O., Turbulence, An Introduction to Its Mechanism and Theory, McGraw-Hill Book Co., 1959.

10. Holman, J. P., Heat Transfer, 2nd Ed., McGraw-Hill Book Co., 1963.

11. Householder, M. K., and Goldschmidt, V. W., "Turbulent Diffusion of Small Particles in a Two Dimensional Free Jet," Report Submitted to the Nat. Sci. Foundation, Tech. Rpt. FMTR-68-3, Purdue Research Foundation 5307, pp. 132-143, 1968.

12. Jenkins, P. E., "A Study of the Intermittent Region of a Heated Two-Dimensional Plane Jet," Ph. D. Thesis, Purdue University, December, 1974.

13. Kaiser, K. F., "An Experimental Investigation of the interaction of an Acoustic Field," MS Thesis, Purdue University, January, 1971.

14. Kibens, V., "The Intermittent Region of a Turbulent Boundary Layer," Ph. D. Thesis, The John Hopkins University, 1968.

15. Kovasznay, L. S. G., Kibens, V., and Blackwelder, R. F., "Large Scale Motion in the Intermittent Region of a Turbulent Boundary Layer," J. Fluid Mech. Vol. 41, Part 2, pp. 283-325, 1970.

16. Miller, D. R. and Commings, B. W., "Static Pressure Distribution in the Free Turbulent Jet," J. Fluid Mech. Vol. 3, Part 1, pp. 1-16, October, 1957.

17. Oswald, L. J. and Kibens, V., "Turbulent Flow in the Wake of a Disk," Technical Report, The University of Michigan, 1971.

18. Ott, E. S., III, "Convective Velocities in a Turbulent Plane Jet," MS Thesis, Purdue University, December, 1972.

19. Paizis, S. T. and Schwarz, W. H., "An Investigation of the Topography and Motion of the Turbulent Interface," J. Fluid Mech. Vol. 63, Part 2, pp. 315-343, 1974.

20. Phillips, O. M., "The Entrainment Interface," J. Fluid Mech. Vol.51, Part 1, pp. 97-118, 1972.

21. Schlichting, H., Boundary Layer Theory, 6th Ed., McGraw-Hill Book Co., 1968.

22. Taylor, G. I., "Statistical Theory of Turbulence," Proceedings of the Royal Society of London, Series A, Part 1, pp. 421-444, 1935.

23. Thomas, R. M., "Conditional Sampling and Other Measurements in a Plane Turbulent Wake," J. Fluid Mech. Vol. 57, Part 3, pp. 549-582, 1973.

24. Townsend, A. A., "Local Isotropy in the Turbulent Wake of a Cylinder," Australian Jour. Sci. Res. Series A, Vol. 2, pp. 161-174, 1948.

25. Townsend, A. A., "The Fully Developed Turbulent Wake of a Circular Cylinder, " Australian Jour. Sci. Res. Series A, Vol. 2, pp. 451-468, 1949.

26. Townsend, A. A., The Structure of Turbulent Shear Flow, Cambridge University Press, 1956.

27. Townsend, A. A., "The Mechanism of Entrainment in Free Turbulent Flows," J. Fluid Mech. Vol. 26, Part 4, pp. 689-715, 1966.

28. Van der Hegge Zinjen, B. G., "Measurements of Heat and Matter in a Plane Turbulent Jet of Air," Appld. Sci. Res. Vol. 7, Section A, pp. 277-292, 1957.

29. Young, M. F., "A Turbulence Study: Convective Velocities, Energy Spectra, and Turbulence Scales in a Plane Air Jet," MS Thesis, Purdue University, August, 1973.

GENERAL REFERENCES

1. Brodkey, R. S., The Phenomena of Fluid Motions, Addison-Wesley Publishing Co., 1967.

2. Holman, J. P., Experimental Methods for Engineers, 2nd Ed., McGraw-Hill Book Co., 1971.

3. La Rue, J. C., "The Temperature Characteristics in the Turbulent Wake of a Heated Rod," Ph. D. Thesis, University of California, San Diego, 1973.

4. Sandborn, V. A., Resistance Temperature Transducers, Metrology Press, 1972.

5. Tennekes, H. and Lumley, J. L., A First Course in Turbulence, The MIT Press, 1972.

APPENDICES

APPENDIX A THE DESIGN OF A LOW SPEED WIND TUNNEL

This appendix is meant to document the work done by the author in the design and construction of a low speed wind tunnel. The purpose of the wind tunnel is to be part of an experimental setup for taking mean and conditional measurements of temperature and velocity in the cold wake of a cylinder.

The final design of the wind tunnel's test section is shown in Figure A-1, and Figures A-2, A-3 and A-4 show the actual wind tunnel built by the shop staff of the Herrick Laboratories.

The test section has a cross section of 30.48 x 45.72 cm wide and 2.44 m in length. One side of the test section is made of 1.91 cm plexiglas with a 1.27 cm slot at the midplane of the tunnel. The slot is to be used to insert probes into the flow field.

The tunnel was designed as an open loop wind tunnel with the blower at the exit, sucking the air through the tunnel. This was done to achieve the best results with a minimum of cost and labor.

A tunnel such as the one built will have a relatively low turbulent intensity level in the test section without the need for screens, straws or honeycombs. This was the major reason for the choice.

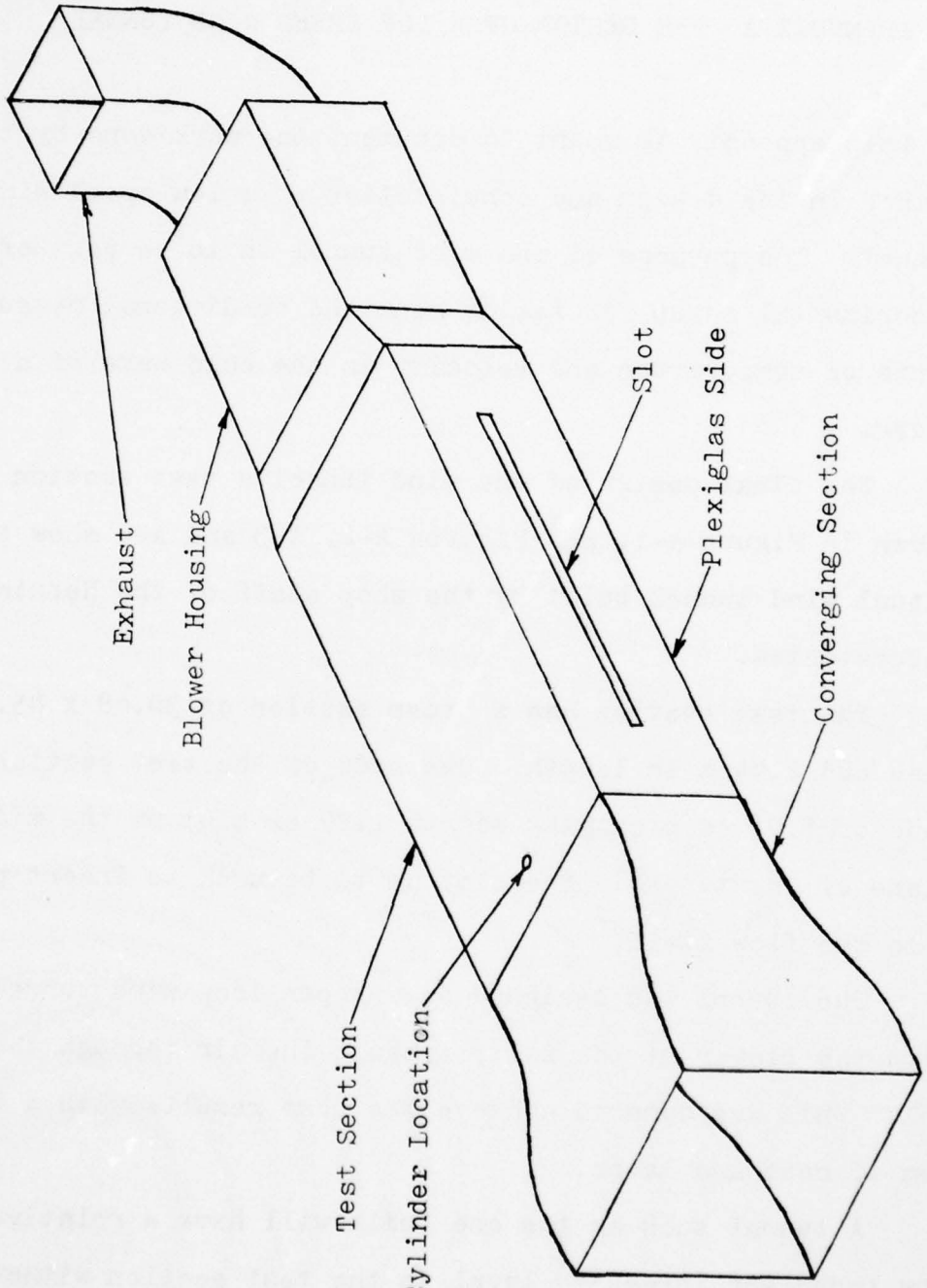

Figure A-1 Schematic of Wind Tunnel

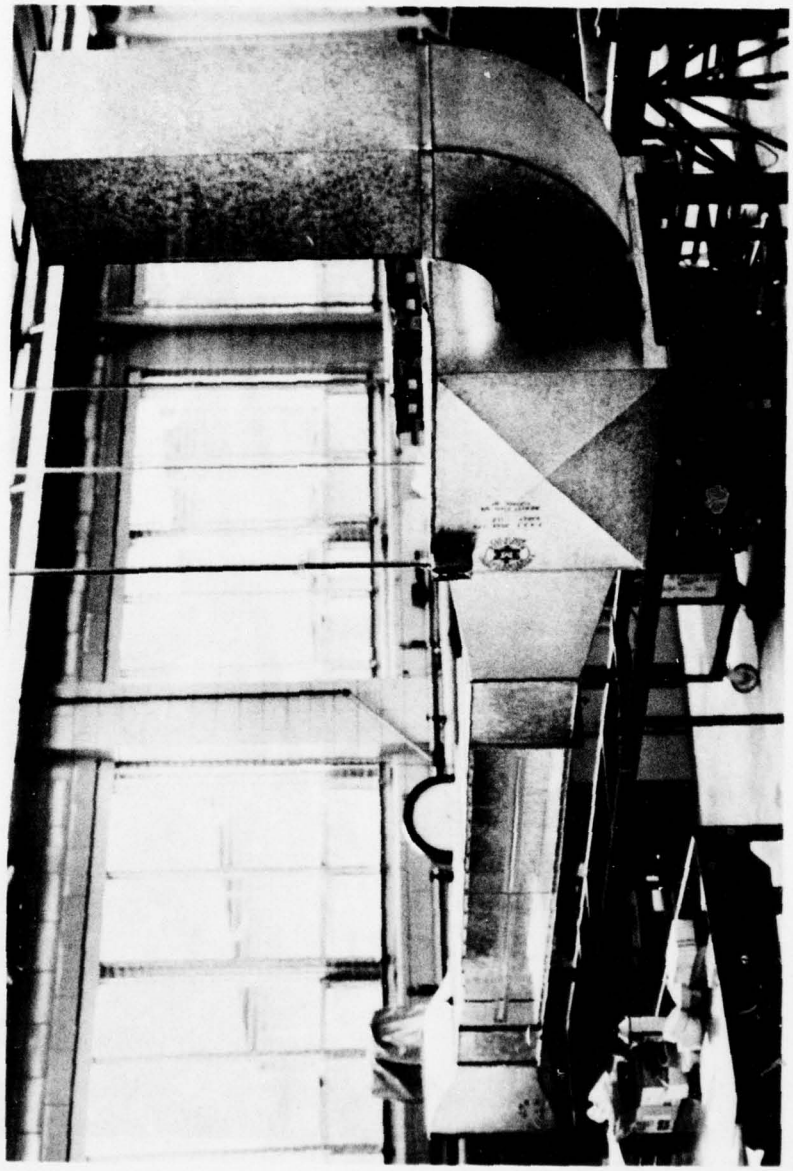

Figure A-2 Wind Tunnel Setup

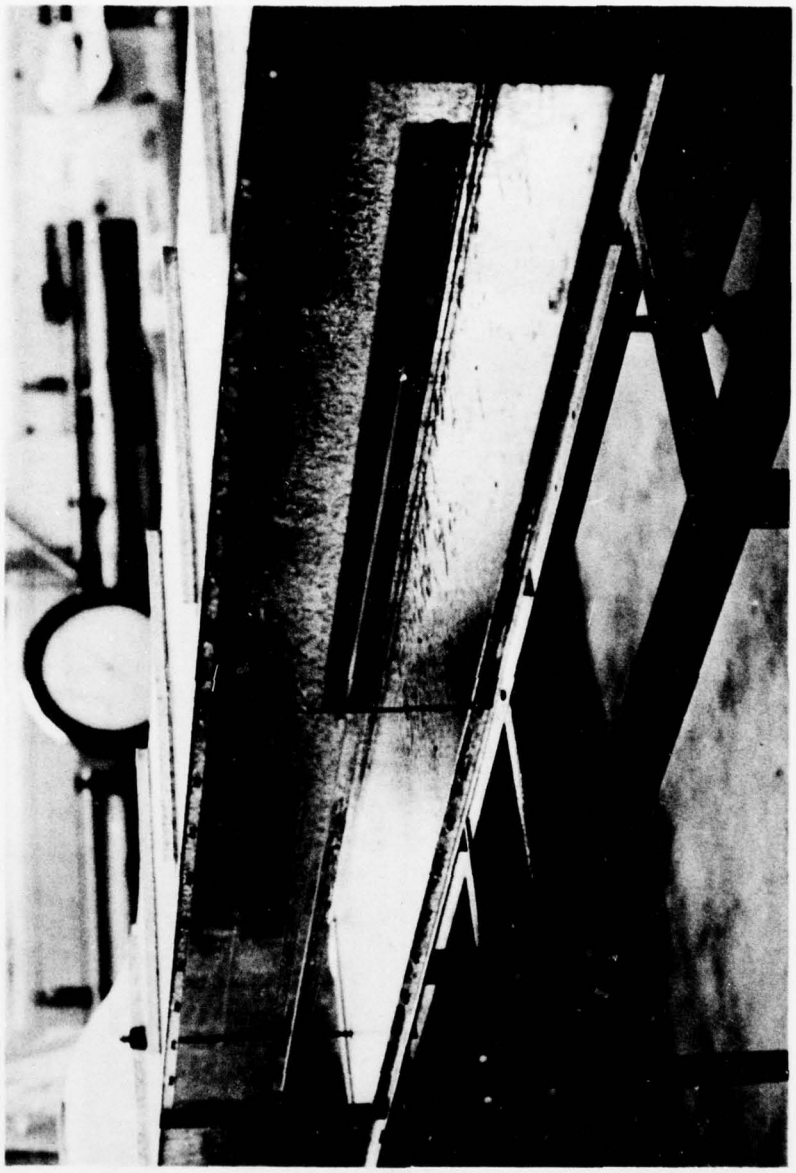

Figure A-3 Wind Tunnel Test Section

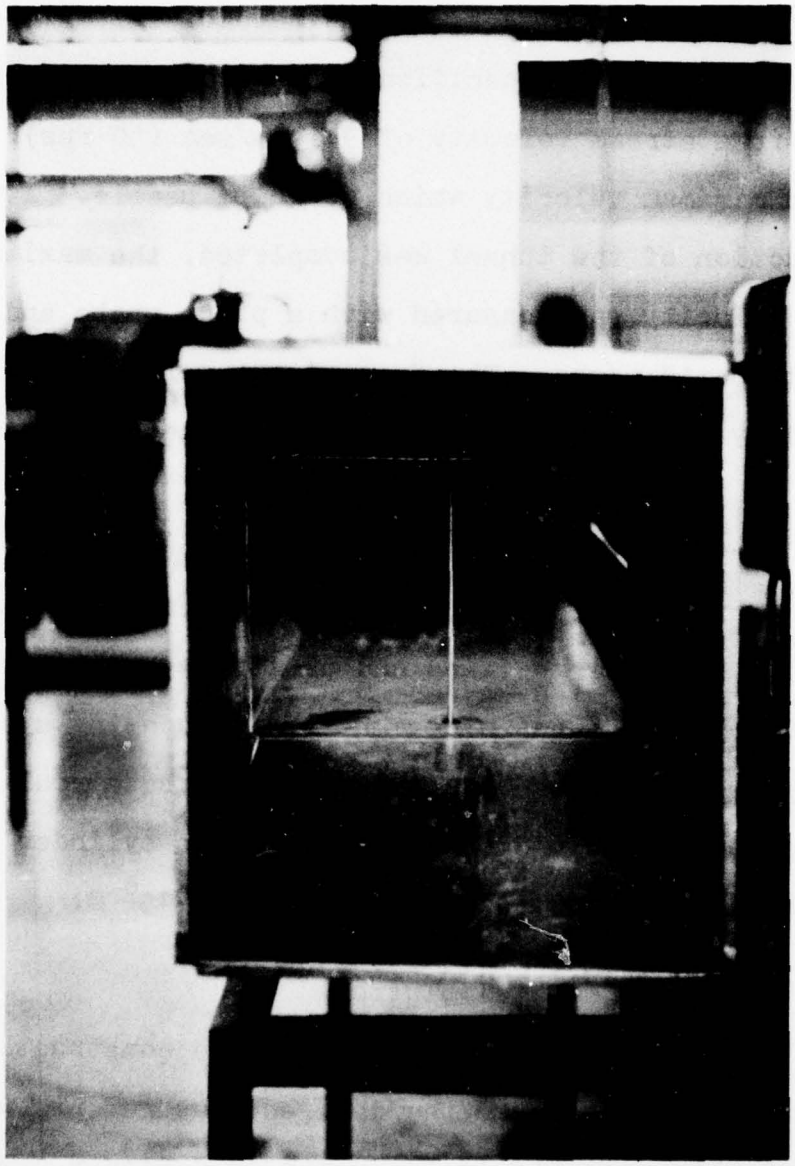

Figure A-4 View of Inlet to Wind Tunnel

The tunnel is equipped with a LAU blower, model A10-10 AC, squirrel cage type. It is powered by a 1.12 kW motor rated at 3450 RPM.

In the design stages, a flow rate of 1.7 m^3/sec (3600 cfm) was chosen as a specification so that the tunnel would have a free stream velocity of 9.14 m/sec (30 fps). This was the minimum velocity which would be usable. After the construction of the tunnel was completed, the maximum free stream velocity was measured with a pitot probe and was found to be 10 m/sec. The free stream velocity can be controlled by a flapper valve that covers the exhaust of the blower.

Since the wind tunnel was meant to be used to take measurements in the wake of a cooled circular cylinder, a cooling system was designed and partially built for the tunnel. Figure A-5 shows a design for the cooling system. It is proposed that Freon 502 (BP = -45° C) be circulated through the system and hence maintain the cylinder within the tunnel at a constant temperature of -45° C.

Calculations

Calculations were made prior to the construction of the wind tunnel to make sure the desired measurements would be theoretically possible in the setup as designed. The calculations will be reviewed here.

To establish Reynolds number similarity, Townsend (1956) has found practically no effect on the mean velocity profiles

Note: All surfaces outside the test section are to be insulated.

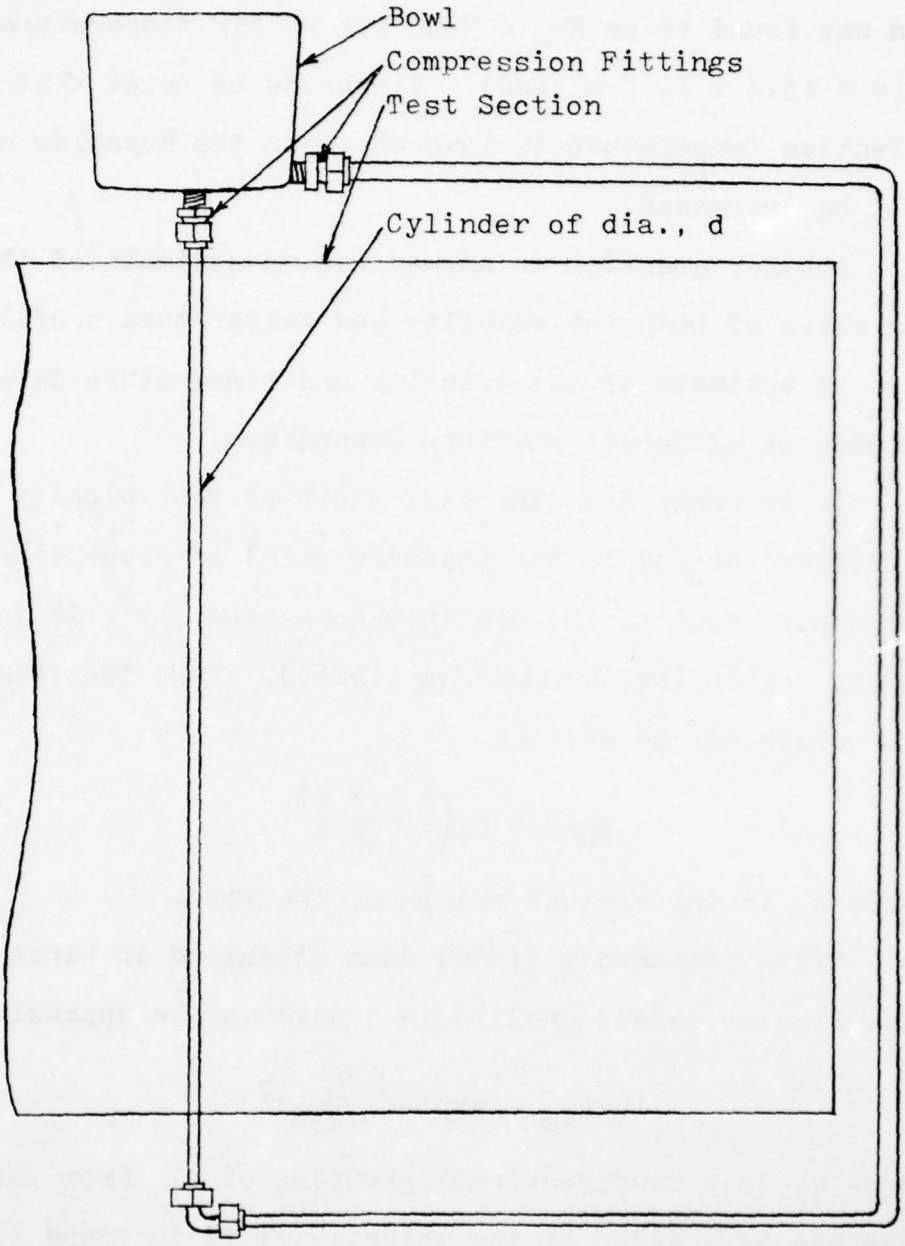

Figure A-5 Schematic of Cylinder Cooling System

when $Re_d > 800$. The Reynolds number based on the cylinder diameter was calculated with $\bar{U}_o = 9.14$ m/sec and d = 0.635 cm and was found to be $Re_d = 3800$ for an air temperature of 23° C ($\nu = 15.2 \times 10^{-6}$ m^2/sec). It should be noted that if the effective temperature is lowered, then the Reynolds number will be increased.

Another question to answer was an estimate of the widening rates of both the velocity and temperature profiles, and also an estimate of the velocity and temperature defect magnitudes at different stations downstream.

It is known that the half width of the velocity field, b_u, (where db_u/dx is the widening rate) is proportional to the square root of the distance downstream, $x^{\frac{1}{2}}$, in the similarity region (see Schlichting (1968)). Thus the form of the half width may be written

$$b_u/d = C_1\left(\frac{x - x_o}{d}\right)^{\frac{1}{2}} \qquad \text{(A-1)}$$

where x_o is the virtual origin of the wake.

Using Townsend's (1949) data discussed in Hinze (1959), the velocity defect profile in a wake may be approximated by

$$\bar{U}_1/\bar{U}_{1m} = \exp(-(\frac{\eta_2}{0.256})^2) \qquad \text{(A-2)}$$

where η_2 is a nondimensional grouping of y. From this equation the half width of the velocity field is found to be

$$b_u/d = 0.213\left(\frac{x + a}{d}\right)^{\frac{1}{2}} \qquad \text{(A-3)}$$

Making the assumption that the same virtual origin will exist in the designed test setup as was found by Townsend in

his experimental work (a/d = 20), it is possible to estimate the half width of the wake as a function of the distance downstream. The widening rate of the velocity field is shown in Figure A-6.

In a similar fashion the half width of the temperature field in the wake of a circular cylinder will have the form

$$b_\theta/d = C' \left(\frac{x - x'_o}{d} \right)^{\frac{1}{2}} \qquad \text{(A-4)}$$

From the temperature measurements taken by Townsend (1949) and analyzed by Hinze (1959), it has been found that a reasonable fit to the data is obtained from a model based on a constant coefficient of thermal transport. From this model the temperature profile is a Gaussian solution similar to the velocity profile,

$$\theta/\theta_m = \exp\left(-\left(\frac{\eta_2}{0.348}\right)^2\right) \qquad \text{(A-5)}$$

The widening rate of the temperature field may then be found to be

$$b_\theta/d = 0.290 \left(\frac{x + a}{d} \right)^{\frac{1}{2}} \qquad \text{(A-6)}$$

By making the same assumptions concerning the virtual origins of the wake, an estimate of the spreading rate of the temperature may be found. The widening rate of the temperature profile is shown in Figure A-6. The two widening rates are shown together for the sake of comparison. The figure shows the temperature spreading faster that the mean velocity. This difference in spreading rates has been

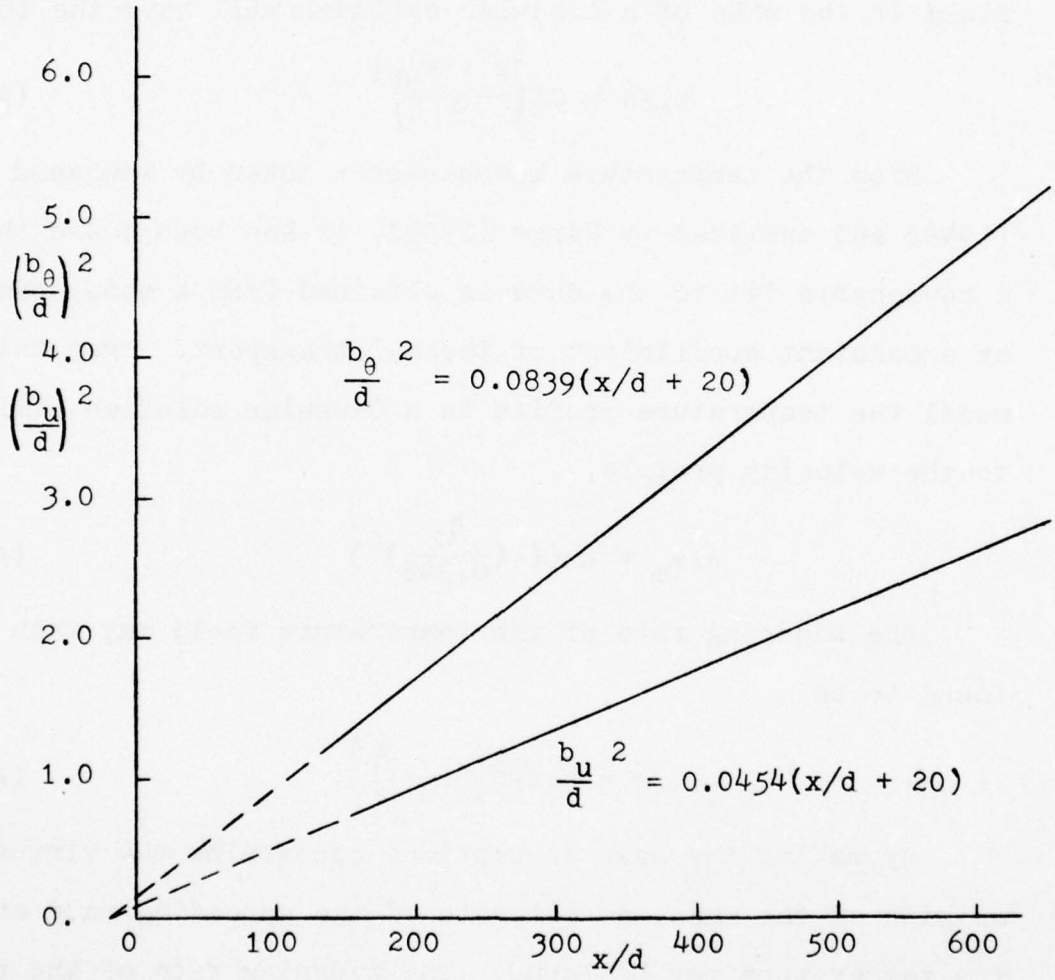

Figure A-6 Predicted Widening Rates of Velocity and Temperature Profiles

explained by Jenkins (1974) for a plane jet to be caused by the different slopes of the point averaged velocity and temperature profiles ($d\hat{\bar{\theta}}/dy$ and $d\hat{\bar{U}}/dy$) at the interface.

It is also desired to estimate the velocity and temperature defects on the centerline of the wake as a function of the distance downstream. According to Schlichting (1968), the centerline velocity defect varies with the distance downstream as

$$U_{1m}/U_o = k\left(\frac{x + a}{d}\right)^{-\frac{1}{2}} \qquad \text{(A-7)}$$

in the similarity region. From data taken by Townsend (1956) the velocity defect relationship may be approximated as

$$U_o/U_{1m} = 1.09(x/d - 25)^{\frac{1}{2}} \qquad \text{(A-8)}$$

Since no data was readily available, the temperature defect at the centerline, θ_m, was approximated by forming an energy balance. The heat out of the system is found by the heat transfer to an infinite cylinder in a crossflow situation. The Reynolds number based on the diameter of the cylinder and the bulk temperature of the fluid is 5300. From Holman (1968) the Nusselt number relation corresponding to the Reynolds number range is given as

$$Nu_d = 0.174(Re_d)^{0.618} \qquad \text{(A-9)}$$

For the given flow situation the Nusselt number is 38.1, which corresponds to a heat flux per unit length of

$$Q_{out} = 167.3 \quad (W/m) \qquad \text{(A-10)}$$

The heat flux into the system comes from the entrainment of ambient fluid into the wake. Across a slice of the flow, the heat flux is given by

$$Q_{in} = \int_{-\infty}^{\infty} \rho U c_p \theta dy \qquad \text{(A-11)}$$

where U is the velocity of the fluid in the x direction and θ is the temperature defect.

By using the definition of velocity defect, $U_1 = U_o - U$, and assuming the velocity and temperature defect profiles may be described as Gaussian solutions,

$$U_1 = U_{1m} \exp(-\alpha^2 y^2) \qquad \text{(A-12a)}$$

$$\theta = \theta_m \exp(-\beta^2 y^2) \qquad \text{(A-12b)}$$

with $\alpha = \sqrt{\ln 2}/b_u$ and $\beta = \sqrt{\ln 2}/b_\theta$, we may solve for θ_m.

Combining these equations, the heat flux into the system is

$$Q_{in} = \rho c_p U_o \theta_m \int_{-\infty}^{\infty} e^{-\beta^2 y^2} dy - \rho c_p U_{1m} \theta_m \int_{-\infty}^{\infty} e^{-(\alpha^2+\beta^2) y^2} dy \qquad \text{(A-13)}$$

The solution of (A-13) gives

$$Q_{in} = \rho c_p \theta_m \sqrt{\pi} \left(\frac{U_o}{\beta} - \frac{U_{1m}}{\gamma} \right) \qquad \text{(A-14)}$$

where $\gamma = (\alpha^2 + \beta^2)^{\frac{1}{2}}$.

The heat flux in and out of the system may be equated, since the flow is assumed steady and there are no losses. Equating (A-10) and (A-14), gives an expression containing θ_m,

$$\theta_m = \frac{167.3}{\rho c_p \sqrt{\pi} \left(\frac{U_o}{\beta} - \frac{U_{1m}}{\gamma} \right)}$$

$$\theta_m = 0.0783\left(\frac{U_o}{\beta} - \frac{U_{1m}}{\gamma}\right)^{-1} \qquad \text{(A-15)}$$

The temperature defect along the centerline of the wake may be estimated from (A-15). This is shown in Figure A-7 along with the velocity defect along the centerline of the wake.

Conclusions

A sample of some of the results that may be obtained from the above calculations are found in Table A-1. Case I of the table was taken as a standard set of variables which might be used in the wind tunnel. Case II shows what changes might be expected as a result of changing the cylinder diameter from 0.635 cm to 0.318 cm. Case III shows what changes might occur with a change of cooling agents (from Freon 502, BP = -45° C to liquid N_2, BP = -195.8° C).

The information which can be gained from these calculations, given a set of variables is:

1. What is the maximum x/d station at which measurements may be taken?
2. At x/d_{max}, what is the width of the velocity and temperature field? Will there be any interference from the sides of the wind tunnel?
3. At x/d_{max}, what is the magnitude of the velocity defect and the temperature difference? Can these magnitudes be measured accurately?

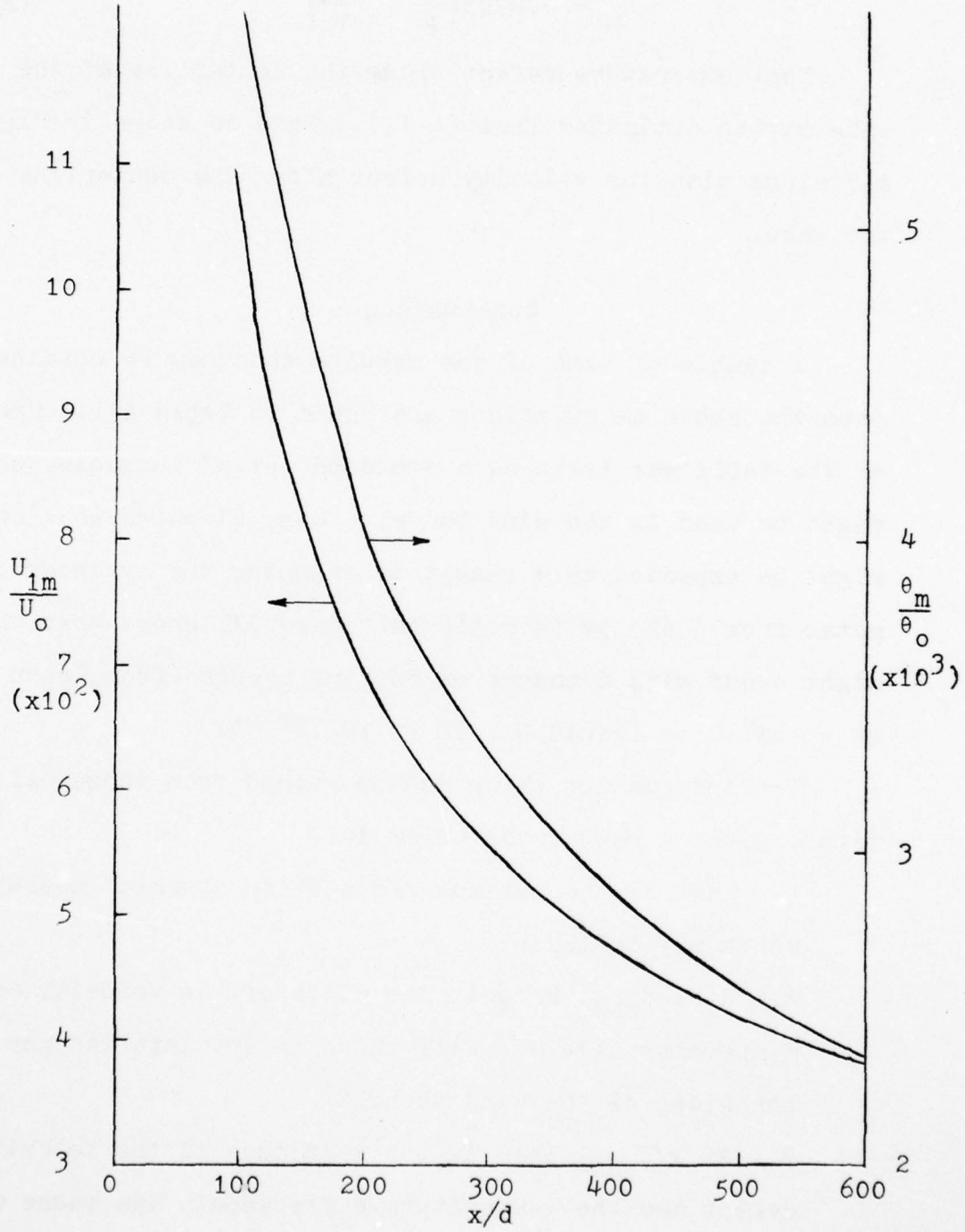

Figure A-7 Predicted Centerline Velocity and Temperature Defects vs. x/d

Table A-1 Predicted Results for Wind Tunnel

Control Variables	Case I	Case II	Case III
U_o (m/sec)	9.14	9.14	9.14
θ_o (^{o} C)	67.8	67.8	218.3
d (cm)	0.635	0.318	0.635
Parameters			
Re_d	5300	2700	8800
x/d_{max}	360	700	360
x_{max} (m)	2.29	2.23	2.29
Predicted Measurements @ x/d_{max}			
b_u (cm)	2.64	1.82	2.64
b_θ (cm)	3.59	2.47	3.59
U_{1m} (m/sec)	0.458	0.323	0.458
θ_m (^{o} C)	0.205	0.294	0.660

AD-A066 186 PURDUE UNIV LAFAYETTE IND RAY W HERRICK LABS F/G 20/4
VELOCITY AND FOLDOVER OF THE TURBULENT NON-TURBULENT INTERFACE --ETC(U)
SEP 75 D J MULEJ, V W GOLDSCHMIDT N00014-75-C-1048

UNCLASSIFIED HL-75-32 NL

2 OF 2
ADA
066186

END
DATE
FILMED
5-79
DDC

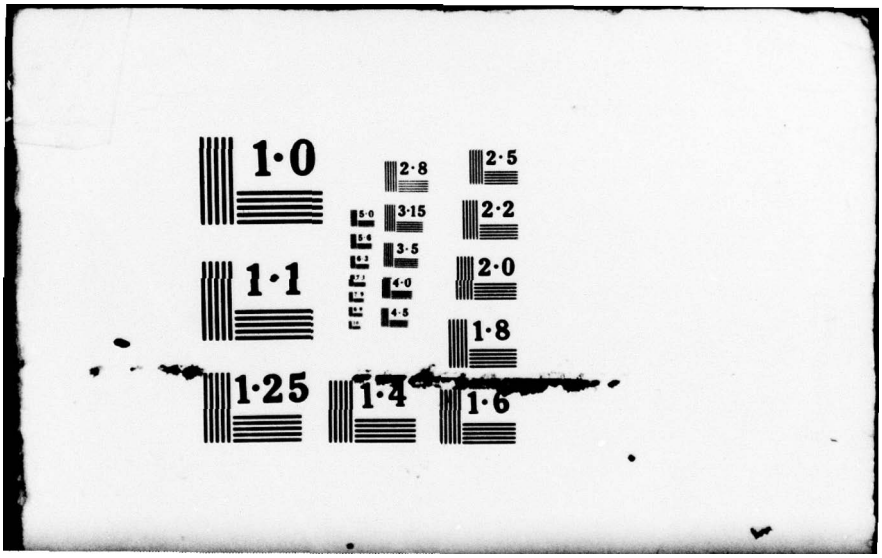
1·0
1·1
1·25
2·8
3·15
3·5
4·0
4·5
2·5
2·2
2·0
1·8
1·4
1·6

APPENDIX B CONDITIONAL MEASUREMENT OF Λ

This appendix is intended to present the preliminary results of an attempt to measure the point averaged lateral space scales in a two dimensional plane jet. It is intended to discuss the circuitry necessary to measure the point averaged space correlation, to show the preliminary results obtained at one location in the jet, and to discuss the significance of the proposed measurements.

A point averaged measurement is a special type of conditional measurement. When the interface is sensed to be in a predetermined position a sample from another probe is taken. The average of a large number of these samples is a point averaged value. It is recognized as the mean value in the fully turbulent region, at a specified distance from the interface, when the interface is in a predetermined position.

Measurement Procedure

Figure B-1 shows a schematic of the procedure used for measuring the mean space correlation, g(r), and the point averaged correlation coefficient. It shows the signals taken from two hot wire probes (see Figures 11 and 12 for positioning of the probes), which are separated by a distance, r, in the lateral direction. These signals are amplified, AC

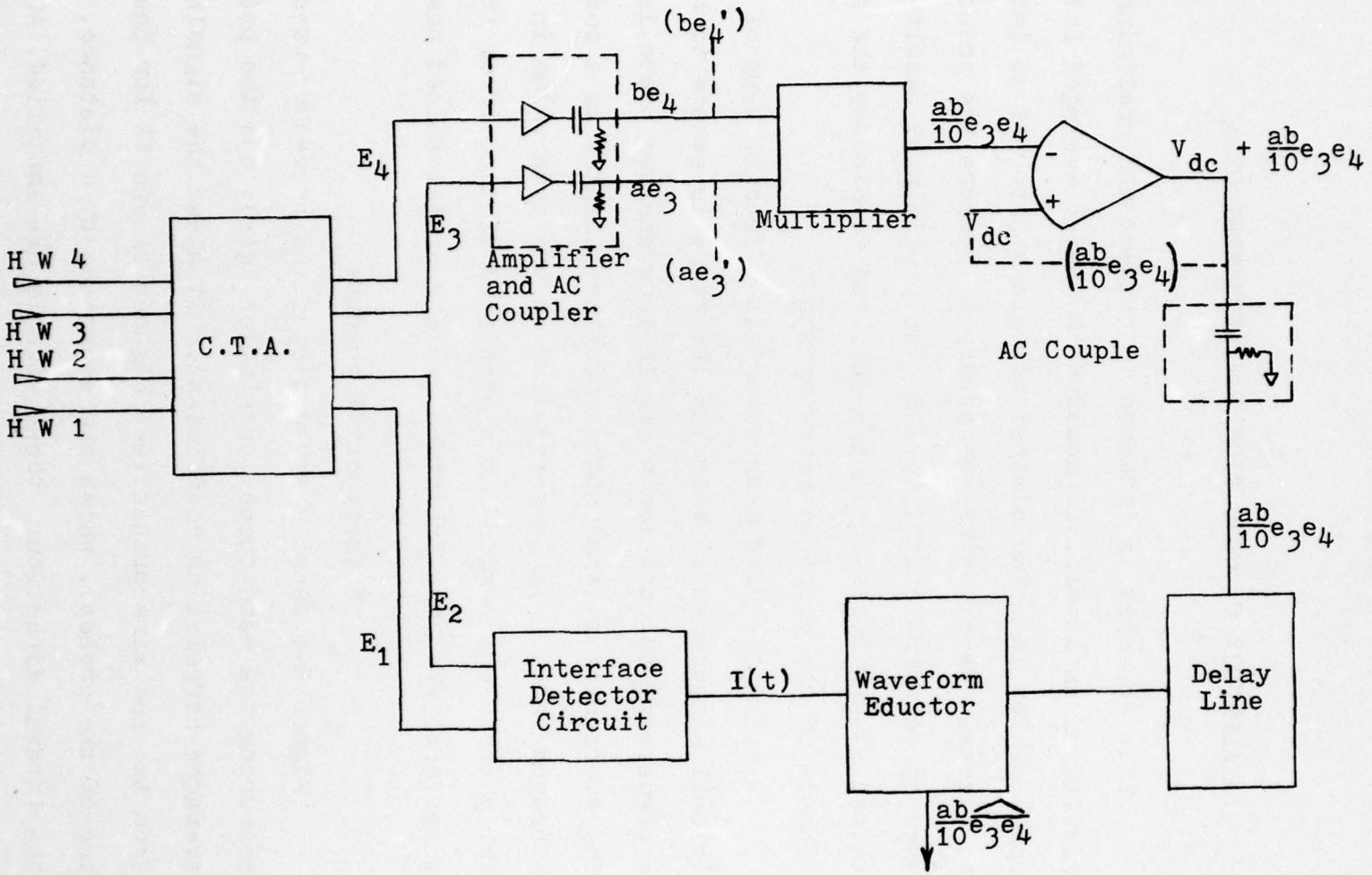

Figure B-1 Schematic of Λ Measurement Process

coupled, and finally multiplied together using an Analog Devices multiplier circuit, model 426 K. The conditioned signal is then biased by a known constant DC voltage and measured using a B & K RMS meter and CALICO digital voltmeter.

The lateral space correltation coefficient, g(r), is defined by Taylor (1935) as

$$g(r) = \frac{\overline{u(\xi_1)u(\xi_1+r)}}{u'(\xi_1)u'(\xi_1+r)} \qquad \text{(B-1)}$$

This is equivalent to

$$g(r) = \frac{\overline{e_3 e_4}}{e_3' e_4'} \qquad \text{(B-2)}$$

where e_3 and e_4 are the voltage fluctuations corresponding to the velocity fluctuations, $u(\xi_1)$ and $u(\xi_1+r)$ respectively. Thus from the schematic the correlation coefficient may be obtained from the measurement of ae_3', be_4' and $\frac{ab}{10}\overline{e_3 e_4}$ as

$$g(r) = 10\left(\frac{\frac{ab}{10}\overline{e_3 e_4}}{ae_3' be_4'}\right) \qquad \text{(B-3)}$$

The lateral space macroscale, Λ_g, is defined as

$$\Lambda_g = \int_0^\infty g(r)dr \qquad \text{(B-4)}$$

As a means to establish a precedent the macroscale in this work will be measured as

$$\Lambda_g = \int_0^{r'} g(r)dr$$

where $g(r') = 0$, since the possiblity exists for g(r) to be a negative value. This relieves the ambiguity of the definition (B-4).

The signal from the voltage summer, $V_{dc} + \frac{ab}{10}e_3e_4$, is AC coupled to eliminate the bias voltage and put into the variable time delay before going to the Waveform Eductor. The purpose of introducing a delay time is to match the delay time introduced by the interface detector circuit.

The signal I(t) which triggers the Waveform Eductor comes from the interface detector circuit and the two hot wire detector probes. The output of the detector is a signal, I(t), which is unity when the flow seen by the detector probes is turbulent and zero when the flow is nonturbulent. The time derivative of I(t) will give a nonzero reading at the times when the interface is crossing the detector probes. The intricacies of the interface detector circuit are discussed thoroughly by Jenkins (1974).

When the Waveform Eductor triggers on the signal I(t), a sample of the signal (in this case $\frac{ab}{10}e_3e_4$) is taken. After an appropriate number of samples is taken and averaged, the result is $\frac{ab}{10}\widehat{e_3e_4}$, the point averaged value of $\frac{ab}{10}e_3e_4$.

The point averaged correlation coefficient, $\hat{g}(r)$, is defined as

$$\hat{g}(r) = \frac{\widehat{e_3e_4}}{\hat{e}_3'\hat{e}_4'} \qquad \text{(B-6)}$$

where $\hat{e}_3'$ and $\hat{e}_4'$ are the root mean squared values of the values $\hat{e}_3$ and $\hat{e}_4$ (ie. from $\hat{E} = \hat{\bar{E}} + \hat{e}$). The circuitry to make these measurements has not been assembled, although it should not be difficult to do using digital techniques.

In order to approximate the point averaged lateral space scale, an approximate point averaged correlation coefficient, $\hat{g}_1(r)$, is defined as

$$\hat{g}_1(r) = \frac{\widehat{e_3 e_4}}{\overline{e_3 e_{4max}}} \tag{B-7}$$

and then the approximate point averaged lateral scale will be given by

$$\hat{\Lambda}_{g1} = \int_o^{r'} \hat{g}_1(r)dr \tag{B-8}$$

To form an idea of the validity of this approximation, the same approximation is made with regard to the mean correlation coefficient. That is

$$g_1(r) = \frac{\overline{e_3 e_4}}{\overline{e_3 e_{4max}}} \tag{B-9}$$

will be used to define an approximate lateral space macroscale,

$$\Lambda_{g1} = \int_o^{r'} g_1(r)dr \tag{B-10}$$

which will be compared to Λ_g. This will give some basis to judge the accuracy of the approximation, $\hat{\Lambda}_{g1}$.

Preliminary Results

There is some preliminary data to report. The measurements described above were made at position in a two dimensional plane jet ($x/D = 35$ and $y/b = 1.65$).

Figure B-2 shows a comparison of the mean lateral macroscale and the approximate macroscale. Although these are preliminary results, it does not seem that Λ_{g1} agrees very well with Λ_g.

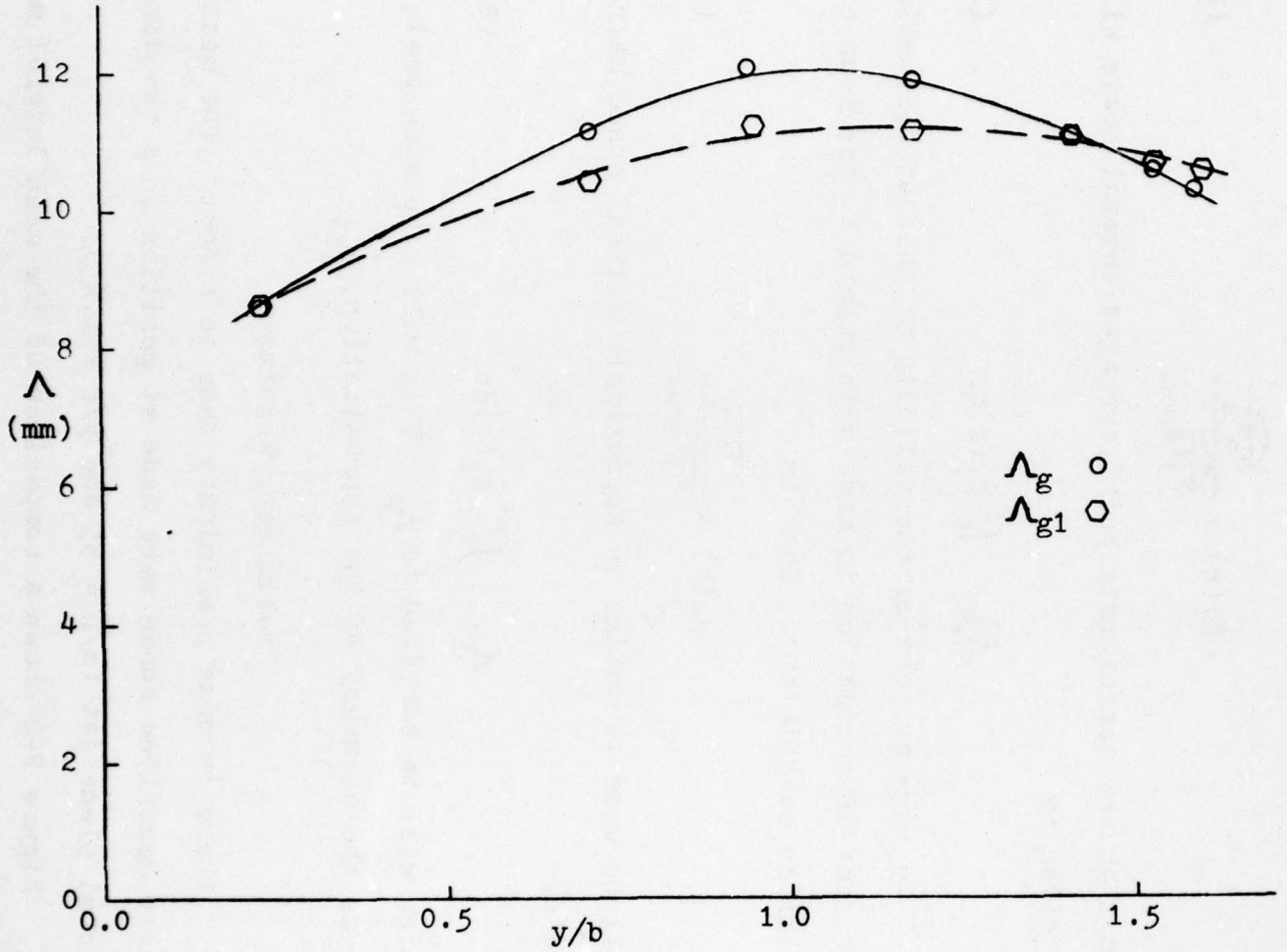

Figure B-2 Λ_g and Λ_{g1} vs. y/b at x/D = 35

APPENDIX C EXAMPLE OF PROCEDURE USED TO DETERMINE V_i FROM DATA

This appendix will show the steps taken to determine V_i from the raw data taken from the visicorder traces. As an example the actual data for one point in the flow field, x/D = 35 and y/b = 2.25, will be analyzed. Table C-2 shows the raw data as it was taken from the visicorder traces.

The average time increments, $\overline{\Delta t}_f$ and $\overline{\Delta t}_b$, are found as the arithmetic mean of the samples and $\overline{\Delta t}$ is given as

$$\overline{\Delta t} = \tfrac{1}{2}(\overline{\Delta t}_f + \overline{\Delta t}_b)$$

The corresponding velocities, V_{fi}, V_{bi}, and V_i can then be computed as a function of the probe separation. These values are shown in Table C-1.

Table C-1 Measured Values of $\overline{\Delta t}$ and $V(\Delta y)$ at x/D = 35 and y/b = 2.25

Δy (mm)	2.5	5.1	7.6
$\overline{\Delta t}_f$ (msec)	1.07	3.20	3.60
$\overline{\Delta t}_b$	2.25	3.53	3.78
$\overline{\Delta t}$	1.66	3.36	3.69
V_{fi} (m/s)	2.37	1.58	2.12
V_{bi}	1.13	1.44	2.01
V_i	1.53	1.51	2.07

Table C-2 Raw Data Taken From Visicorder Traces at x/D = 35 and y/b = 2.25

Δy = 2.5 mm		Δy = 5.1 mm		Δy = 7.6 mm	
Δt_f (mm)	Δt_b (mm)	Δt_f (mm)	Δt_b (mm)	Δt_f (mm)	Δt_b (mm)
0.9	0.9	2.9	3.9	3.6	4.0
1.4	0.7	5.0	2.0	3.1	4.3
0.6	0.8	2.1	7.0	1.4	0.9
0.9	1.1	1.2	-0.1	3.3	3.0
1.3	0.9	1.9	0.7	6.6	1.2
0.3	2.6	5.6	4.0	1.0	5.9
1.1	2.0	2.0	1.0	3.0	1.1
0.3	1.1	2.0	4.9	2.1	1.5
0.0	0.9	4.2	0.4	2.2	3.0
1.9	2.1	2.0	5.1	2.9	5.6
1.1	3.3	-1.0	5.1	1.9	2.0
2.9	5.1	1.8	5.2	1.0	5.9
0.3	0.9	3.0	2.0	3.0	1.8
-1.2	0.9	6.0	1.8	2.7	0.6
1.0	2.0	1.3			
0.0	2.9	1.4			
0.0		2.0			
-1.1		1.0			
3.0		2.4			
0.9					
2.0					
time scale 0.01 sec = 7.84 mm		7.70 mm		7.70 mm	

The velocities shown in Table C-1 are then extrapolated to a zero probe separation. The velocity with $\Delta y = 0.0$ is defined as the velocity at a point in the flow field (i.e. $x/D = 35$ and $y/b = 2.25$). Figure C-1 shows the extrapolation of the velocities to $\Delta y = 0.0$, and also the values of the velocities.

All the velocities discussed in this work were measured in the manner described in this appendix.

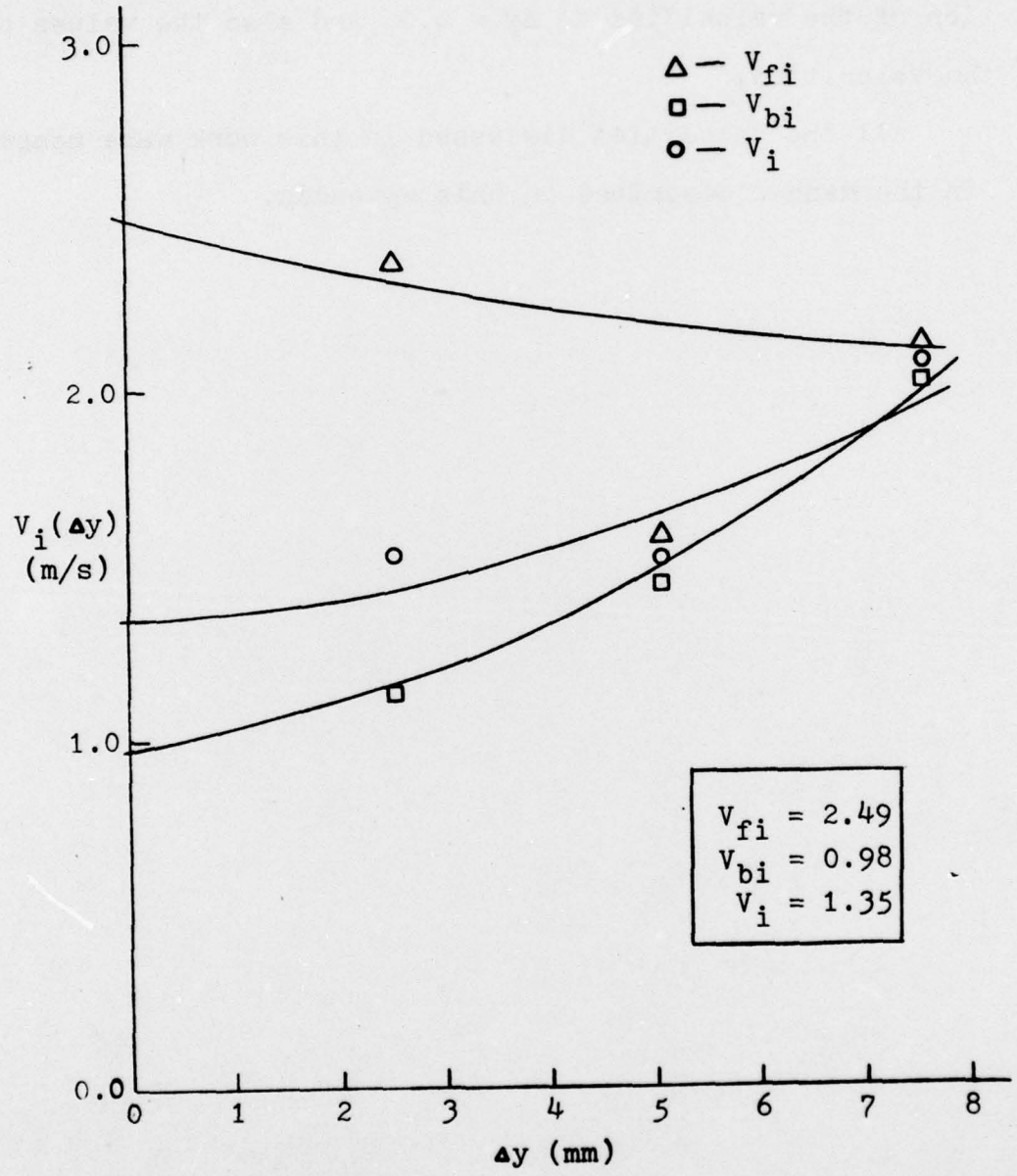

Figure C-1 $V_i(\Delta y)$ vs. Δy